Linköping Studies in Science and Technology Dissertation No. 1629

Synthesis of ZnO and transition metals doped ZnO nanostructures, their characterization and sensing applications

Chan Oeurn Chey

Linköping University
INSTITUTE OF TECHNOLOGY

Physical Electronics and Nanotechnology
Department of Science and Technology
Campus Norrköping, Linköping University
SE-601-74 Norrköping, Sweden
www.liu.se

Synthesis of ZnO and transition metals doped ZnO nanostructures, their characterization and sensing applications

Chan Oeurn Chey

ISBN: 978-91-7519-206-2
ISSN 0345-7524

chan.oeurn.chey@liu.se
chanoeurn@rupp.edu.kh

Linköping University
Department of Science and Technology
SE-601-74 Norrköping, Sweden
Printed by LiU-Tryck, Linköping 2015

Dedicated to:
My family and the soul of my Father

Abstract

Nanotechnology is a technology of the design and the applications of nanoscale materials with their fundamentally new properties and functions. Nanosensor devices based on nanomaterials provide very fast response, low-cost, long-life time, easy to use for unskilled users, and provide high-efficiency.

1-D ZnO nanostructures materials have great potential applications in various sensing applications. ZnO is a wide band gap (3.37 eV at room temperature) semiconductor materials having large exciton binding energy (60 meV) and excellent chemical stability, electrical, optical, piezoelectric and pyroelectric properties. By doping the transition metals (TM) into ZnO matrix, the properties of ZnO nanostructures can be tuned and its room temperature ferromagnetic behavior can be enhanced, which provide the TM-doped ZnO nanostructures as promising candidate for optoelectronic, spintronics and high performance sensors based devices. The synthesis of ZnO and TM-doped ZnO nanostructures via the low temperature hydrothermal method is considered a promising technique due to low cost, environmental friendly, simple solution process, diverse 1-D ZnO nanostructures can be achieved, and large scale production on any type of substrate, and their properties can be controlled by the growth parameters. However, to synthesize 1-D ZnO and TM-doped ZnO nanostructures with controlled shape, structure and uniform size distribution on large area substrates with desirable properties, low cost and simple processes are of high interest and it is a big challenge at present.

The main purpose of this dissertation aims to develop new techniques to synthesize 1-D ZnO and (Fe, Mn)-doped ZnO nanostructures via the hydrothermal method, to characterize and to enhance their functional properties for developing sensing devices such as biosensors for clinical diagnoses and environmental monitoring applications, piezoresistive sensors and UV photodetector.

The first part of the dissertation deals with the hydrothermal synthesis of ZnO nanostructures with controlled shape, structure and uniform size distribution under different conditions and their structural characterization. The possible parameters affecting the growth which can alter the morphology, uniformity and properties of the ZnO nanostructures were investigated. Well-aligned ZnO nanorods have been fabricated for high sensitive piezoresistive sensor. The development of creatinine biosensor for clinical diagnoses purpose and the development of glucose biosensor for

indirect determination of mercury ions for an inexpensive and unskilled users for environmental monitoring applications with highly sensitive, selective, stable, reproducible, interference resistant, and fast response time have been fabricated based on ZnO nanorods.

The second part of the dissertation presents a new hydrothermal synthesis of (Fe, Mn)-doped-ZnO nanostructures under different preparation conditions, their properties characterization and the fabrication of piezoresistive sensors and UV photodetectors based devices were demonstrated. The solution preparation condition and growth parameters that influences on the morphology, structures and properties of the nanostructures were investigated. The fabrication of Mn-doped-ZnO NRs/PEDOT:PSS Schottky diodes used as high performance piezoresistive sensor and UV photodetector have been studied and Fe-doped ZnO NRs/FTO Schottky diode has also been fabricated for high performance of UV photodetector. Finally, a brief outlook into future challenges and relating new opportunities are presented in the last part of the dissertation.

Keywords: Synthesis ZnO nanostructures, TM-doped ZnO NRs, Hydrothermal method, Biosensors, Piezoresistive sensors, UV photodetectors, Diluted magnetic semiconductors.

Acknowledgement

Many people have been involved in helping me to complete this dissertation. My gratitude is beyond words. It is really a pleasant task to express my thanks to all those who contributed in various ways to the success of my PhD study and made it a memorable experience for me.

First of all, I would like to express my gratitude to my supervisor Prof. Magnus Willander for his endless guidance, support, motivation, encouragement, and patient help during my PhD study. Thank you very much for giving me this wonderful opportunity. Under your guidance and encouragement I successfully surpassed many difficulties and learned a lot. You have given enough freedom during my research to encourage me becoming an independent thinker. You are a great supervisor.

I would also like to express my sincere thanks to my co-supervisor, Assoc. Prof. Omer Nour for his valuable discussion, constructive suggestions, contributions, help, patience, and endless support.

I express my deepest gratitude to all my co-authors who shared with me the stressful times and supported me with their knowledge.

I would like to express my gratitude to our research administrator Ann-Christin Norén for her kind and patient help in my work and life. Thank you Ann-Christin for all your support.

I am thankful to the Physical Electronics and Nanotechnology group members for their moral support, best wishes, and unforgettable times we spent together in Norrköping.

I am thankful to International Science Programme (ISP) of Uppsala University for providing financial support during my PhD study; I owe very especial thanks to Assoc. Prof. Ernst van Groningen, Director of Physics Program and Assoc. Prof. Carla Puglia, Assistant Director of Physics Program for their motivation, support and encouragement.

I would like to express my gratitude to all ISP administrator staffs Mr. Hossein Aminaey, Dr. Tore Hållander, Dr. Peter Roth, Ms. Pravina Gajjar, Ms. Therese Rantakokko, and Ms. Zsuzsanna Kristófi for their kind, support and patient help during my study.

For my family, words cannot describe my gratitude. I am grateful to my entire family for their sincere love; I pay high regards to my brother Chey Thavy and his family. I am thankful for your sincere encouragements and inspirations throughout my study. I also express my appreciation to all my in-laws family for their love and encouragement for my PhD study.

Last but not least, my wife, Chanthoubopha, words are not enough to express my gratitude for you. Thank you for love and patience. I appreciate my beloved sons Vatdanak and Bandeth Vichea, who have made our life full of joy with their innocent acts and refreshing me with lovely smiles, why-why questions and kisses.

List of publications included in this dissertation

I. **Chan Oeurn Chey**, Hatim Alnoor, Mazhar Ali Abbasi, Omer Nur and Magnus Willander, "Fast synthesis, morphology transformation, structural and optical properties of ZnO nanorods grown by seed-free hydrothermal method", *Phys. Status Solidi A* **211**, No. 11 (2014) 2611-2615.

Contribution: Most of the experimental work, except CL measurement. Wrote the first draft of the manuscript and contributed to the final editing of the manuscript.

II. **Chan Oeurn Chey**, Hatim Alnoor, Xianjie Liu, Mazhar Ali Abbasi, Omer Nur and Magnus Willander, "ZnO nanorods based piezoresistive sensor synthesized by rapid mixing hydrothermal method", ***(Submitted to Sensors and Actuators A: Physical).***

Contribution: Most of the experimental work, except CL and XPS measurements. Wrote the first draft of the manuscript and contributed to the final editing of the manuscript.

III. **Chan Oeurn Chey**, Syed M. Usman Ali, Zafar H. Ibupoto, Kimleang Khun, Omer Nur and Magnus Willander, "Potentiometric creatinine biosensor based on ZnO nanowires", *J. Nanosci. Lett.* **2012**, 2:24 (2012) 6 pages.

Contribution: All experimental work. Wrote the first draft of the manuscript and contributed to the final editing of the manuscript.

IV. **Chan Oeurn Chey**, Zafar Hussain Ibupoto, Kimleang Khun, Omer Nur and Magnus Willander, "Indirect determination of mercury ion by inhibition of a glucose biosensor based on ZnO nanorods", *Sensors* **2012**, 12 (2012) 15063-15077.

Contribution: All experimental work. Wrote the first draft of the manuscript and contributed to the final editing of the manuscript.

V. **Chan Oeurn Chey**, Omer Nur and Magnus Willander, "Low temperature aqueous chemical growth, structural, and optical properties of Mn-doped ZnO nanowires", *Journal of Crystal Growth* **375** (2013) 125-130.

Contribution: Most of the experimental work, except PL and XPS measurements. Wrote the first draft of the manuscript and contributed to the final editing of the manuscript.

VI. **Chan Oeurn Chey**, Xianjie Liu, Hatim Alnoor, Omer Nur and Magnus Willander, "Fast piezoresistive sensor and UV photodetector based on Mn-doped ZnO nanorods", *Phys. Status Solidi (RRL)* (2014) 1-5, DOI:10.1002/pssr.201409453.

Contribution: Most of the experimental work, except XPS measurement. Wrote the first draft of the manuscript and contributed to the final editing of the manuscript.

VII. **Chan Oeurn Chey**, Ansar Masood, A. Riazanova, Xianjie Liu, K.V. Rao, Omer Nur, and Magnus Willander, "Synthesis of Fe-doped ZnO nanorods by rapid mixing hydrothermal method and its application for high performance UV photodetector", *Journal of Nanomaterials***, Volume 2014**, Article ID 524530 (2014) 9 pages.

Contribution: Most of the experimental work, except SQUID and XPS measurements. Wrote the first draft of the manuscript and contributed to the final editing of the manuscript.

List of publications not included in this dissertation

I. S. M. Usman Ali, Z. H. Ibupoto, **C. O. Chey**, O. Nur and M. Willander, "Functionalized ZnO nanotube arrays for the selective determination of uric acid with immobilized uricase", *Chemical Sensors* **2011** (2011) 1:19.

II. Z. H. Ibupoto, S. M. Usman Ali, **C. O. Chey**, K. Khun, O. Nur, and M. Willander, "Selective zinc ion detection by functionalised ZnO nanorods with ionophore", *Journal of Applied Physics* **110** (2011) 104702.

III. Z. H. Ibupoto, S. M. Usman Ali, K. Khun, **C. O. Chey**, O. Nur and M. Willander, "ZnO nanorods based enzymatic biosensor for selective determination of penicillin", *Biosensors* **2011, 1** (2011) 153-163.

IV. K. Khun, Z. H. Ibupoto, S. M. Usman Ali, **C. O. Chey**, O. Nur and M. Willander, "Ion sensor based on functionalized ZnO nanorods", *Electroanalysis* **22** (2012) 521-528.

V. K. Khun, Z.H. Ibupoto, **C. O. Chey**, J. Lu, O. Nur, M. Willander, "Comparative study of ZnO nanorods and thin films for chemical and biosensing applications and the development of ZnO nanorods based potentiometric strontium ion sensor", *Applied Surface Science* **268** (2013) 37-43.

VI. **C. O. Chey**, H. K. Patra, M. Tengdelius, M. Golabi, O. Parlak, R. Imani, Sami A. I. Elhag, W. Yandi, and A. Tiwari, "Impact of nanotoxicology towards technologists to end users", *Tutorial Article, Adv. Mat. Lett.* **4(8)** (2013) 591-597.

VII. A. Echresh, **C. O. Chey**, M. Z. Shoushtari, O. Nur and M. Willander, "Tuning the emission of ZnO nanorods based LEDs using Ag doping", *Journal of Applied Physics* **116**, (2014) 193104.

VIII. A. Echresh, **C. O. Chey**, M. Z. Shoushtari, O. Nur and M. Willander, Effect of doping on the efficiency of light emitting diode based on the n-ZnO nanorods/p-GaN heterojunction under forward and reverse bias. *Journal of Luminescence* ***(Accepted).***

IX. A. Echresh, **C. O. Chey**, M. Z. Shoushtari, V. Khranovskyy, O. Nur and M. Willander, UV photo-detector based on p-NiO thin film/n-ZnO nanorods heterojunction prepared by a simple process, *Journal of Alloys and Compounds*, ***(Accepted).***

X. E. S. Nour, **C. O. Chey**, M. Willander and O. Nur, A flexible anisotropic self-powered piezoelectric direction sensor based on double sided ZnO nanowires configuration ***(Submitted to IOP-Nanotechnology).***

XI. H. Alnoor, **C. O. Chey**, V. Khranovskyy, M. Eriksson, O. Nur, and M. Willander, Effect of precursors (Zn:HMTA) molar ratio on low temperature hydrothermal synthesis of iron ZnO nanorods and their effects on morphology, structural and optical properties. ***(Manuscript).***

Conference papers

I. **C. O. Chey**, S. M. U. Ali, Z. H. Ibupoto, C. Sann, K. Khun, K. Meak, O. Nur, and M. Willander, "Fabrication and characterization of light emitting diodes based on n-ZnO nanotubes grown by a low temperature aqueous chemical method on p-GaN", CLMV-02, 11-15 October 2011, Vietnam.

II. S. M. U. Ali, **C. O. Chey**, Z. H. Ibupoto, C. Sann, and M. Willander, "Fabrication and characterization of heterojunction light emitting diode based on n-ZnO nanoporous structure grown on p-GaN", CLMV-02, 11-15 October 2011, Vietnam.

III. S. M. U. Ali, **C. O. Chey**, Z. H. Ibupoto, M. Kashif, K. Khun , U. Hasim, and M. Willander, "Selective determination of cholesterol using functionalized ZnO nanotubes based sensor", CLMV-02, 11-15 October 2011, Vietnam.

IV. F. Mahmood, S. M. U. Ali, **C. O. Chey**, H. Ing, and M. Willander, "Design of broadband monopole antenna for mobile handsets", CLMV-02, 11-15 October 2011, Vietnam.

V. **C. O. Chey**, O. Nur, and M. Willander, "Surface-morphology evolution of ZnO nanostructures by influence of ethanol content in low temperature hydrothermal synthesis", Conference on Advanced Functional Materials (AFM2014), 20-21 August 2014,Vildmarkshotellet Kolmården, Norrköping, Sweden.

List of Figures

List of Tables

Table of Contents

Chapter 1: Introduction

1.1 Nanotechnology and nanomaterials

1.1.1 Nanotechnology and applications

Nanotechnology is the creation and exploitation of nanomaterials with structural features in between those of atoms and their bulk materials. In order words, nanotechnology is a technology of design and applications of nanoscale materials with their fundamentally new properties and functions. When the dimensions of materials are in nanoscales the properties of the materials are significantly different from those of atoms as well as those of bulk materials. Moreover, when the size of materials is in the nanoscale regime the large surface area to volume ratio exhibited by nanomaterials, improves the high surface reactivity with the surrounding surface, which makes nanomaterials ideally suitable candidates for many types of sensor applications. Therefore, nanomaterials has opened up possibilities for new innovative functional devices and technologies [1-2]. The importance of nanotechnology was pointed out by Richard Feynman in his delivered lecture at an international forum in the meeting of the American Physical Society at California Institute of Technology (CalTech) entitled ‘‘There is plenty of room at the bottom’’ on 29 December 1959 [3]. Currently, nanotechnology has been recognized as a revolutionary field of science and technology and have been applied in many applications, including environmental applications, medical applications, biomedical applications, healthcare and life sciences, agricultures, food safety, security, energy production and conversion applications, energy storage, consumer goods, infrastructure, building and construction sector, and aerospace [4-7]. Moreover, the new nanotechnology applications provide very fast response, low-cost, long-life time, easy to use for unskilled users, and high-efficiency of devices and it also provides a new approaches to diagnosis and treatment of diseases, effective environmental monitoring and alternative ways for substantial energy development for a better world. We can say that, nanotechnology is applied almost in every aspect of our modern world.

In this regard, the development of new methods to synthesize nanomaterials have paved the way in creating new opportunities for the development of innovative nanostructures based devices. In particular, the ability to synthesize nanostructures materials with controllable shape, size and structure and enhance the properties of nanomaterials provides excellent prospects for designing nanotechnology based devices.

1.1.2 Classification and synthesis of nanomaterials

Over decades, the ability to tune surface morphologies and the structure of semiconductor materials with near atomic scale has led to further idealization of semiconductor structures: quantum wells, wires, and dots. These nanostructures have completely different density of electronic states predicted by simple particle in a box type models of quantum mechanics. According to their basic dimensions (X, Y and Z) in space, nanostructures of nanomaterials can be classified into zero-dimension (0-D), one-dimension (1-D), two-dimension (2-D) and three-dimension (3-D). While 0-D nanostructures refer to quantum dots or nanoparticles, 1-D nanostructures refer to nanowires, nanorods, nanofibres, nanobelts, and nanotubes, 2-D nanomaterials represent for nanosheets, nanowalls and nanoplates and 3-D nanomaterials are nanoflowers and other complex structures such as nanotetrapods [8-12]. Due to the quantum effects dominating most of the properties of the nanomaterials, its density of states of the nanomaterials are quite different from those of the bulk materials. The density of states which describes the electronic states versus energy in the band diagram of the 0-D, 1-D, 2-D and bulk materials are shown in Figure 1.1.

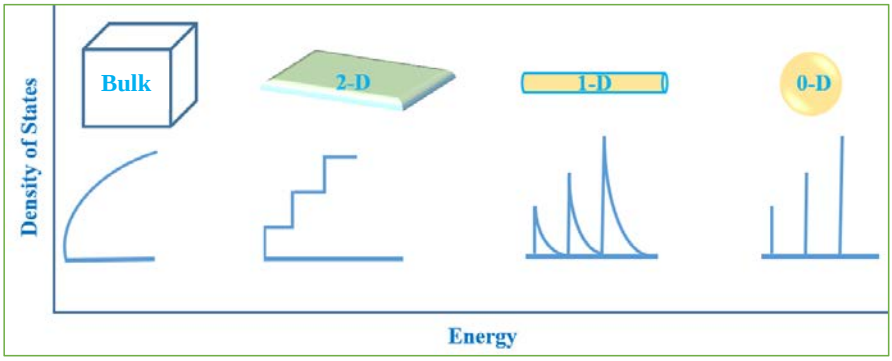

Figure 1. 1: *The electron density of states in bulk semiconductor and the electron density of states in quantum well (2-D), in quantum wire (1-D), and in quantum dot (0-D) nanomaterials (adopted from [8, 12]).*

Nanotechnology fields have extensive research focused on gaining control of particle size, shape, and composition in different ways. However, syntheses of nanoscale materials are generally grouped into mainly two approaches: bottom-up and top-down approaches. The bottom up method is a method that build nanomaterials from atomic or molecular precursors while top-down technique is a method that tearing down larger building blocks into finer pieces till their constitution up to nanoscale level. The schematic diagram of these two approaches are presented in Figure 1. 2.

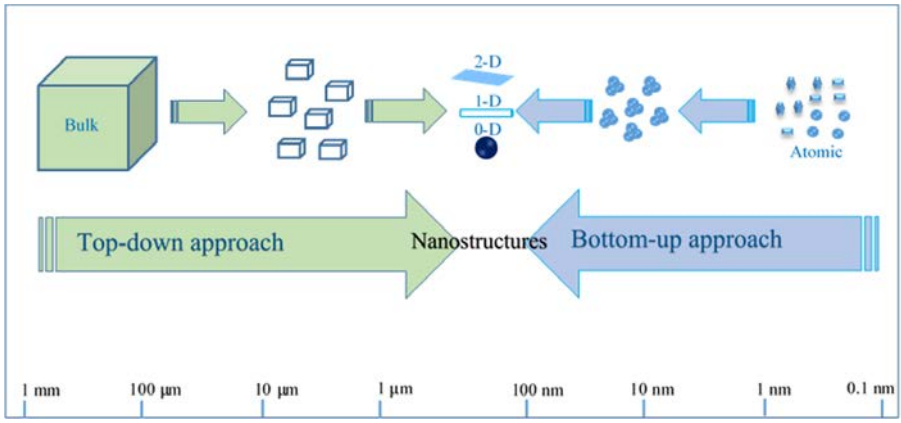

Figure 1. 2: *Top-down and bottom-up approaches (adopted from [14]).*

1.2 Background of sensors and nanomaterials

As a sensor is a device that senses a change in a physical conditions (forces) or chemical quantities or biological quantities which produces a measurable response signal to a specific measurable input [15-16]. A sensor's physical configuration consists of a sensing element together with its physical packaging and external connections [17]. The schematic diagram of sensor system is shown in Figure 1.3.

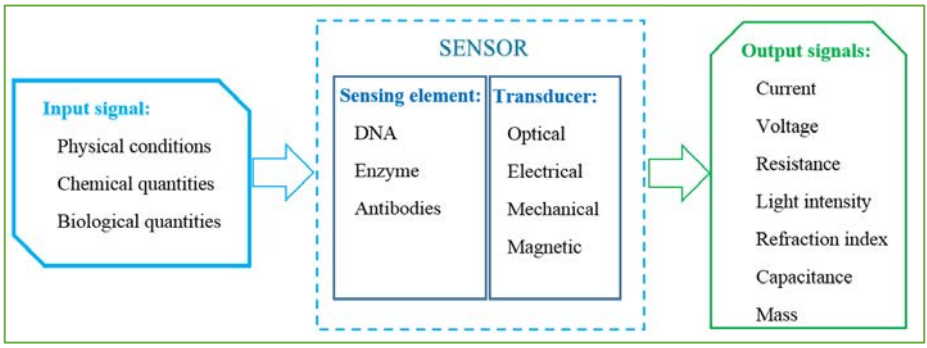

Figure 1. 3: *Schematic diagram of a sensor system.*

Many attractive features of nanostructured materials are interested for sensing applications. These is due to quantum confinement effects in semiconductor nanostructures, the ability to tailor the size, structure and properties. Furthermore, nanostructured materials possess excellent electrical, optical, thermal, catalytic properties and strong mechanical strength, which offers great opportunities to construct nanomaterials-based sensors and excellent prospects for designing novel sensing systems [18-20]. The reason is that reducing

the size of nanomaterials led to increase the surface area to volume ratio, which increases the activities between materials and its surrounding environment. This phenomena caused the sensor increased sensitivity, improved detection limits, provide faster responses and smaller amounts of samples can be measurable with lower cost, easy to use for unskilled users, high-efficiency and less power consumption.

1.3 Sensing applications based on ZnO and TM-doped ZnO nanostructures

In recent years, nanomaterial-based sensors have attracted much attention from both scientific research communities and from industrial applications points-of-view. For sensor applications, the fabrication processes are on economic oriented approach, use of inexpensive materials by economical synthesis methods and the sensor system should presents low power consumption, ease of fabrication, high accuracy, fast response time, high compatibility, portable and easy to use for unskilled users are the most important factors for the development of new sensors based devices. In the response to above requirements, metal oxide semiconductor nanomaterials have attracted high interest due to their promising applications in a diversity of technological areas, including sensors area. In the fields of nanotechnology based sensors, metal oxides nanostructures stand out as being among the most versatile nanomaterials because of their excellent physical and chemical properties [21-22]. Among metal oxide nanomaterials, ZnO nanostructures are of the most promising metal oxides due to their attractive physical and chemical properties. From these properties, ZnO nanostructures are highly attractive from research communities in the applications of sensing. ZnO nanomaterials have attracted huge attention in sensing areas due to its relatively large surface area to volume ratio, larger band gap (3.37 eV at room temperature), high exciton binding energy (60 meV) which makes excitons in ZnO stable up to 350 K, high transparency, its high ionicity and biocompatibility [21-29]. Also, ZnO is an important multifunctional material suitable for many different applications in transparent electronics, optoelectronics, transparent electronics, solar cell, smart windows, biodetection, piezoelectric devices [30-33]. In addition, the performance of the sensors can be improve by doping ZnO nanostructure with different metals or by alloyed ZnO with other metal oxides. This is due to the dopant influenced on the properties ZnO nanostructures such as the band gap, optical property and electrical conductivity [33-39]. Furthermore, room temperature ferromagnetic properties are also achieved by doping with transition metals into ZnO nanostructures, which shows potential for increasing performance of sensing device and for future spintronics applications [40-43]. Among ZnO nanostructures, 1-D ZnO nanostructures such as nanorods, nanowires, nanobelts,

and nanotube are becoming a major focus in nanoscience research and are of interest for many different applications due to their important physical properties and application prospects. The key factors for the great interest in 1-D ZnO nanostructures in sensing applications arises for many reasons. The electron transport in 1-D ZnO nanostructures are directly in contact with the surrounding environment and high surface area to volume ratio which is mandatory for fast reaction kinetics. Their high electronic conductance, minimum power consumption, relatively simple preparation methods and large-scale production can achieved. 1-D ZnO nanostructures have superior stability due to high crystallinity, ultrahigh sensitivity, and the potential for the integration of addressable arrays on a mass production scale. It also exhibits as semiconducting properties and also piezoelectric properties which can form the basis for electromechanically coupled sensors and transducers, it is relatively biocompatible and they can be relatively easily incorporated into microelectronic devices [16, 19, 21 and 24].

The unique properties of 1-D ZnO nanostructures provide promising combination for sensitivity, chemical selectivity, an electronically and chemically tunable platform crucial for tailored sensor response [19, 21]. Therefore, 1-D ZnO nanostructures are important potential candidates for the realization of sensor applications. So far, 1-D ZnO nanostructures, especially ZnO NRs/NWs are extensively applied in various sensing applications fields, e.g. biosensors [44-51], biomarker [52-53], drug delivery [54-55] , chemical sensors [56-58], gas sensors [59-60], pH sensors [61], humidity sensor [62-64], UV sensors [65-69], temperature sensors [70-71], and pressure/force/mass/load sensors [72-75]. Also, the high performances of several types of sensors have been enhanced by utilizing different metals doped ZnO nanorods, e.g. high performance of sensors can be achieved by Cu, Ag or Al-doped ZnO nanorods for UV sensors [76-78], Mg, Au, Al or Cr doped ZnO nanorods for gas sensors [79-82], Cd-doped ZnO nanorods for humidity sensor [83] and Sb-doped ZnO nanobelts for strain sensor [84].

The properties of 1-D ZnO nanostructures rely strongly on their synthesis routes and their structure, surface morphology, chemical composition, surface contamination, electron transport, and other properties which are affecting on the sensing properties. Therefore, 1-D ZnO nanostructures have been synthesized by various methods in order to tailor their properties, including chemical vapor deposition (CVD) [85], metalorganic chemical vapor deposition (MOCVD) [86-87], pulsed laser deposition (PLD) [88], and molecular beam epitaxy (MBE) [89-90]. However, these methods require high temperature, high cost and limit the growth on soft flexible substrates. In order to solve these problems, the “bottom-up” strategy is broadly applicable for synthesizing new materials on any types of substrates and especially, the low temperature hydrothermal approach have been widely used for growing many different

ZnO nanostructures due to many reason, including low cost, simplicity, environmental friendly and easy to scale up. Various nanostructures can be achieved by controlling the hydrothermal growth parameters and preparation conditions. Due to the fact that the properties of 1-D ZnO nanostructures rely on their synthesis route, the surface morphology, size, shape and structures and the chemical bonds play fundamental roles in determining the 1-D ZnO nanomaterials properties and their corresponding sensing applications. Therefore, tailoring properties of 1-D ZnO nanostructures for desirable sensing applications is of high interest to researchers. The controlled preparation of 1-D ZnO nanostructures is considered to play a significant role in exploring the prospects and future challenges for the development of sensing devices. Therefore, this dissertation aims to provide a novel route to the low temperature hydrothermal synthesis of 1-D ZnO and TM-doped ZnO nanostructures with fast, low cost, controllable size, shape, uniform distribution and structure orientation with desirable properties for higher sensor's performances and multifunctional sensing devices.

1.4 Objectives and scope of this study

1.4.1 Dissertation objectives

The main purpose of this dissertation aims to realize controllable synthesis of un-doped ZnO and (Fe, Mn)-doped ZnO nanostructures via the low temperature hydrothermal method, their characterization and enhancing their functional properties for developing new sensing devices, including biosensors, piezoresistive sensors and UV photodetectors and providing new multifunctional sensing platforms. The overall objectives of this dissertation are pursued as the following:

- **Hydrothermal synthesis of ZnO and TM-doped ZnO nanostructures**

The first objective aims to develop the low temperature hydrothermal methods to synthesize a controllable surface morphology, shape, uniform size distribution, structure and properties of un-doped ZnO and TM-doped ZnO nanostructures with low cost, fast, low power consumption and preferable on any type of substrate which leads to enhance the performance of sensors.

- **Characterization of ZnO and TM-doped ZnO nanostructures**

The second objective aims to investigate the properties of the synthesized un-doped ZnO and (Fe, Mn)-doped ZnO nanostructures. Various characterization techniques were applied in order to gain deep understanding of the morphological characteristics, crystallinity, light absorption and emission, chemical composition, and magnetic properties. Finally, to provide

these investigated results with their functionalities for developing their corresponding sensing applications.

- **Sensing applications based on ZnO NRs and (Fe, Mn)-doped ZnO NRs**

The third objective aims to fabricate sensor devices based on the synthesized ZnO NRs and (Fe, Mn)-doped ZnO NRs for chemical, biological, UV and piezoresistive sensing applications. Firstly, due to the piezoresistive effect of ZnO NRs, Au/ZnO NRs Schottky diode has been fabricated using well-aligned and uniform distribution of ZnO NRs grown by rapid mixing synthesis for piezoresistive sensor applications. Secondly, electrochemical sensors have been fabricated by functionalized ZnO NRs for a wide range of detection of creatinine concentration with fast response time. Thirdly, the functionalized ZnO NRs used as a glucose biosensor for indirect determination of environmental mercury ions with very low detection limit and fast response of the biosensor. Finally, high performance piezoresistive sensor and UV photodetector based on PEDOT:PSS/Mn-doped ZnO NRs Schottky diode has been developed and the development of Au/Fe-doped-ZnO NRs Schottky diode has been demonstrated for high performance UV photodetector.

1.4.2. Organization of the dissertation

The dissertation is organized as follow: the general introduction and objective of this research are presented in this chapter 1. Chapter 2 provides basics properties of ZnO and TM-doped ZnO nanostructures for sensing applications, chapter 3 presents background of biosensor, piezoresistive sensor, UV photodetector and their applications based on ZnO and TM-doped ZnO NRs, chapter 4 presents the synthesis methods of ZnO and TM-doped ZnO nanostructures, their characterization techniques and devices fabrication processes, chapter 5 presents the results and discussions and chapter 6 is giving research summary and future prospects.

References

[1] M. C. Roco, C. A. Mirkin, M. C. Hersam, Nanotechnology research directions for societal needs in 2020: summary of international study, *J Nanopart Res* (2011) DOI 10.1007/s11051-011-0275-5.

[2] C. N. R. Rao, A. Muller, A. K. Cheetham, The Chemistry of Nanomaterials, *WILEY-VCH Verlag GmbH & Co. KGaA*, Weinheim, (2004) page 1.

[3] I. P. Kaur, V. Kakkar, P. K. Deol, M. Yadav, M. Singh, I. Sharma, Issues and concerns in nanotech product development and its commercialization, *Journal of Controlled Release*, (2014), http://dx.doi.org/10.1016/j.jconrel.2014.06.005.

[4] P. Boisseau, and B. Loubaton, Nanoscience and nanotechnologies: hopes and concerns nano-medicine, nanotechnology in medicine, *C. R. Physique* **12,** 620-636 (2011).

[5] L. A. DeLouise, Applications of nanotechnology in dermatology, *Journal of Investigative Dermatology* **132**, 964-975 (2012).

[6] S. K. Arora, R. W. Foley, J. Youtie, P. Shapira, and A. Wiek, Drivers of technology adoption- the case of nanomaterials in building construction, *Technological Forecasting & Social Change* **87**, 232-244 (2014).

[7] S. Chattopadhyay, L. C. Chen, and K. H. Chen, Energy production and conversion applications of one-dimensional semiconductor nanostructures, *NPG Asia Mater.* **3**(6), 74-81 (2011).

[8] A. P. Alivisatos, Perspectives on the physical chemistry of semiconductor nanocrystals, *J. Phys. Chem.* **100,** 13226-13239 (1996).

[9] Y. Zhang, M. K. Ram, E. K. Stefanakos, and D. Y. Goswami, Synthesis, characterization, and applications of ZnO Nanowires, *Hindawi Publishing Corporation*, *Journal of Nanomaterials* **2012**, ID 624520 22 pages (2012).

[10] W. Zhao, X. Song, Z. Yin, C. Fan, G. Chen, S. Sun, Self-assembly of ZnO nanosheets into nanoflowers at room temperature, *Materials Research Bulletin* **43**, 3171-3176 (2008).

[11] D. Liu, W. Wu, Y. Qiu, S. Yang, S. Xiao, Q. Q. Wang, L. Ding, and J. Wang, Surface functionalization of ZnO nanotetrapods with photoactive and electro-active organic monolayers, *Langmuir* **24,** 5052-5059 (2008).

[12] http://ecee.colorado.edu/~bart/book/book/chapter2/ch2_4.htm, 10 October 2014.

[13] J. A. Rodriguez, and M. F. Garcia, Synthesis, properties, and applications of oxide nanomaterials, *John Wiley & Sons, Inc.*, Hoboken, New Jersey (2007) page 82.

[14] F. C. Adams, and C. Barbante, Nanoscience, nanotechnology and spectrometry, *Spectrochimica Acta Part B* **86**, 3-13 (2013).

[15] M. Swierczewska, G. Liu, S. Lee, and X. Chen, High-sensitivity nanosensors for biomarker detection, *Chem. Soc. Rev.* **41**, 2641-2655 (2012).

[16] R. P. Singh, A. Tiwari, J. W. Choi, and A. C. Pandey, Smart nanomaterials for biosensors, biochips and molecular bioelectronics, smart nanomaterials for sensor application, *Bentham Science Publishers*, 3-41 (2012).

[17] F. Santiago, K. A. Boulais, A. R. Keller, V. H. Gehman Jr., K. J. Long, Nanomaterials for sensor applications, *Proc. of SPIE* **7343**, 73430P 9 pages (2009), doi: 10.1117/12.822602.

[18] S. Su, W. Wu, J. Gao, J. Lu, and C. Fan, Nanomaterials-based sensors for applications in environmental monitoring, *J. Mater. Chem.* **22**, 18101-18110 (2012).

[19] J. Wang, Nanomaterial-based electrochemical biosensors, *Analyst* **130**, 421-426 (2005).

[20] J. T. Devreese, Importance of nanosensors: Feynman's vision and the birth of nanotechnology, *Mater. Res. Soc. Symp. Proc.* **952**, 0952-F01-01(2007).

[21] N. S. Ramgir, Y. Yang, and M. Zacharias, Nanowire-based sensors, *Small*, **6, No. 16,** 1705-1722 (2010).

[22] L. Vines and A. Kuznetsov, Bulk Growth and Impurities, Semiconductor and semimetal: oxide semiconductors, *Elsevier Inc.* (2013), p. 68.

[23] P. R. Solanki, A. Kaushik, V. V. Agrawal, and B. D. Malhotra, nanostructured metal oxide-based biosensors, *NPG Asia Mater.* **3** (1), 17-24 (2011).

[24] Z. L. Wang, and J. Song, Piezoelectric nanogenerators based on zinc oxide nanowire arrays, *Science*, **Vol. 312, No. 5771,** 242-246 (2006).

[25] B. X. Du, Z. Mei, Z. Liu, Y. Guo, T. Zhang, Y. Hou, Z. Zhang, Q. Xue, and A. Yu. Kuznetsov, Controlled growth of high-quality ZnO-based films and fabrication of visible-blind and solar-blind ultra-violet detectors, *Adv. Mater.* **21**, 4625-4630 (2009).

[26] R. Schifano, E. V. Monakhov, U. Grossner, and B. G. Svensson, Electrical characteristics of palladium Schottky contacts to hydrogen peroxide treated hydrothermally grown ZnO, *Applied Physics Letters* **91**, 193507 (2007).

[27] V. Venkatachalapathy, A. Galeckas, I. H. Lee, A. Yu. Kuznetsov, Engineering of nearly strain-free ZnO films on Si (111) by tuning AlN buffer thickness, *Physica B* **407,** 1476-1480 (2012).

[28] N.T. Son, I.G. Ivanov, A. Kuznetsov, B.G. Svensson, Q.X. Zhao, M. Willander, M. N. Morishita, T. Ohshima, H. Itoh, J. Isoya, E. Janzen, R. Yakimova, Common point

defects in as-grown ZnO substrates studied by optical detection of magnetic resonance, *Journal of Crystal Growth* **310**, 1006-1009 (2008).

[29] T. Moe Børseth, B. G. Svensson, A. Yu. Kuznetsov, P. Klason, Q. X. Zhao, and M. Willander, Identification of oxygen and zinc vacancy optical signals in ZnO, *Applied Physics Letters* **89**, 262112 (2006).

[30] J. E. Stehr, S. L. Chen, S. Filippov, M. Devika, N. K. Reddy, C. W. Tu, W. M. Chen, and I. A. Buyanova, Defect properties of ZnO nanowires revealed from an optically detected magnetic resonance study, *Nanotechnology* **24,** 015701 (5pp) (2013).

[31] S. L. Chen, W. M. Chen, and I. A. Buyanova, Slowdown of light due to exciton-polariton propagation in ZnO, *Physical Review B* **83**, 245212 (2011).

[32] W. M. Chen, I. A. Buyanova, A. Murayama, T. Furuta, Y. Oka, D. P. Norton, S. J. Pearton, A. Osinsky, and J. W. Dong, Dominant factors limiting efficiency of optical spin detection in ZnO-based materials, *Applied Physics Letters* **92**, 092103 (2008).

[33] M. Willander, L. L. Yang, A. Wadeasa, S. U. Ali, M. H. Asif, Q. X. Zhao and O. Nur, Zinc oxide nanowires: controlled low temperature growth and some electrochemical and optical nano-devices, *J. Mater. Chem.* **19**, 1006-1018 (2009).

[34] X. J. Wang, I. A. Buyanova, W. M. Chen, M. Izadifard, S. Rawal, D. P. Norton, S. J. Pearton, A. Osinsky, J. W. Dong, and Amir Dabiran, Band gap properties of Zn_{1-x} Cd_xO alloys grown by molecular-beam epitaxy, *Applied Physics Letters* **89**, 151909 (2006).

[35] A. Gorzkowska-Sobas, A. Galeckas, M. F. Sunding, S. Diplas and A. Yu. Kuznetsov, An investigation of Fe-doped ZnO thin films grown by magnetron sputtering, *Phys. Scr.* **T141**, 014004 (7pp) (2010).

[36] T. M. Børseth J. S. Christensen, K. Maknys, A. Hallén, B. G. Svensson, A.Yu. Kuznetsov, Annealing study of Sb^+ and Al^+ ion-implanted ZnO, *Superlattices and Microstructures* **38**, 464-471 (2005).

[37] A. Yu. Azarov, A. Hallén, X. L. Du, P. Rauwel, A. Yu. Kuznetsov, and B. G. Svensson, Effect of implanted species on thermal evolution of ion-induced defects in ZnO, *Journal of Applied Physics* **115**, 073512 (2014).

[38] V. Khranovskyy, U. Grossner, O. Nilsen, V. Lazorenko, G.V. Lashkarev, B. G. Svensson, R. Yakimova, Structural and morphological properties of ZnO:Ga thin films, *Thin Solid Films* **515**, 472-476 (2006).

[39] V. Venkatachalapathy, A. Galeckas, R. Sellappan, D. Chakarov, A. Yu. Kuznetsov, Tuning light absorption by band gap engineering in ZnCdO as a function of MOVPE-synthesis conditions and annealing, *Journal of Crystal Growth* **315**, 301-304 (2011).

[40] C. Liu, F. Yun, H. Morkoc, Ferromagnetism of ZnO and GaN: A review, *Journal of Material Science: Materials in Electronics* **16**, 555-597 (2005).

[41] C. Ronning, P. X. Gao, Y. Ding, and Z. L. Wang, Manganese-doped ZnO nanobelts for spintronics, *Appl. Phys. Lett.* **84**, 783-785 (2004).

[42] S. J. Pearton, D. P. Norton, M. P. Ivill, A. F. Hebard, J. M. Zavada, W. M. Chen, and I. A. Buyanova, Ferromagnetism in transition metal doped ZnO, *Journal of Electronic Materials,* **Vol. 36, No. 4**, 462-471 (2007).

[43] T. Dietl, Dilute magnetic semiconductors: Functional ferromagnets, *Nature Materials* **2**, 646-648 (2003).

[44] M. Willander, O. Nur, M. Q. Israr, One- and two-dimensional nanostructures for chemical and biosensing, *Procedia Engineering* **25**, 745-748 (2011), doi:10.1016/j.proeng.2011.12.183.

[45] M. Willander, P. Klason, L. L. Yang, S. M. Al-Hilli, Q. X. Zhao, and O. Nur, ZnO nanowires: chemical growth, electrodeposition, and application to intracellular nano-sensors, *phys. stat. sol. (c)* **5**, 3076-3083 (2008).

[46] M. M. Rahman, A. J. S. Ahammad, J. H. Jin, S. J. Ahn, and J. J. Lee, A Comprehensive review of glucose biosensors based on nanostructured metal-oxides, *Sensors* **10**, 4855-4886 (2010).

[47] M. H. Asif, F. Elinder, and M. Willander**,** Electrochemical biosensors based on ZnO nanostructures to measure intracellular metal ions and glucose, *J Anal Bioanal Techniques* **S7** (2011) 9 pages, doi:10.4172/2155-9872.S7-003.

[48] R. Yu, C. Pan, and Z. L. Wang, High performance of ZnO nanowire protein sensors enhanced by the piezotronic effect, *Energy Environ. Sci.* **6**, 494-499 (2013).

[49] M. H. Asif, S. M. U. Ali, O. Nur, M. Willander, C. Brännmark, P. Strålfors, U. H. Englund, F. Elinder, and B. Danielsson, Functionalised ZnO-nanorod-based selective electrochemical sensor for intracellular glucose, *Biosensors and Bioelectronics* **25**, 2205-2211 (2010).

[50] R. Yu, C. Pan, J. Chen, G. Zhu, and Z. L. Wang, Enhanced performance of a ZnO nanowire-based self-powered glucose sensor by piezotronic effect, *Adv. Funct. Mater.***23**, 5868-5874 (2013).

[51] M. Willander et al, Applications of Zinc Oxide Nanowires for Bio-photonics and Bio-electronics, *Proc. of SPIE* **7940**, 79400F-1 (2011).

[52] H. Y. Yue et al, ZnO nanowire arrays on 3D hierachical graphene foam: Biomarker detection of Parkinson's disease, *ACS NANO* **8**, 1639-1646 (2014).

[53] G. Shalev, G. Landman, I. Amit, Y. Rosenwaks, and I. Levy, Specific and label-free femtomolar biomarker detection with an electrostatically formed nanowire biosensor, *NPG Asia Materials* **5,** 7 pages (2013), doi:10.1038/am.2012.75.

[54] S. Kishwar, M. H. Asif, O. Nur, M. Willander, and P. O. Larsson, Intracellular ZnO nanorods conjugated with protoporphyrin for local mediated photochemistry and efficient treatment of single cancer cell, *Nanoscale Res Lett*. **5 (10)**, 1669-1674 (2010).

[55] H. Hong, J. Shi, Y. Yang, Y. Zhang, J. W. Engle, R. J. Nickles, X. Wang, and W. Cai, Cancer-targeted optical imaging with fluorescent zinc oxide nanowires, *Nano Lett.* **11**, 3744-3750 (2011).

[56] Z. H. Ibupoto, S. M. U. Ali, K. Khun, and M. Willander, Selective Thallium (I) ion sensor based on functionalised ZnO nanorods, *Journal of Nanotechnology* **2012**, ID 619062 (6 pages) (2012).

[57] M. H. Asif, O. Nur, M. Willander, M. Yakovleva, and B. Danielsson, Studies on Calcium ion selectivity of ZnO nanowire sensors using ionophore membrane coatings, *Research Letters in Nanotechnology* **2008**, ID 701813 (4 pages) (2008).

[58] M. H. Asif, S. M. U. Ali, O. Nur, M. Willander, U. H. Englund, and F. Elinder, Functionalized ZnO nanorod-based selective magnesium ion sensor for intracellular measurements, *Biosensors and Bioelectronics* **26**, 1118-1123 (2010).

[59] M. J. S. Spencer, Gas sensing applications of 1D-nanostructured zinc oxide: Insights from density functional theory calculations, *Progress in Materials Science* **57**, 437-486 (2012).

[60] E. R. Waclawik et al, Functionalised zinc oxide nanowire gas sensors: Enhanced NO_2 gas sensor response by chemical modification of nanowire surfaces, *Beilstein J. Nanotechnol.* **3**, 368-377 (2012).

[61] A. Fulati, S. M. U. Ali, M. Riaz, G. Amin, O. Nur, and M. Willander, Miniaturized pH Sensors Based on Zinc Oxide Nanotubes/Nanorods, *Sensors* **9**, 8911-8923 (2009).

[62] H. T. Hsueh, T. J. Hsueh, S. J. Chang, F. Y. Hung, C. L. Hsu, B. T. Dai, K. T. Lam, and K. H. Wen, A Flexible ZnO nanowire-based humidity sensor, *IEEE Transactions on Nanotechnology* **11**, 520-525 (2012).

[63] S. P. Chang et al, A ZnO nanowire-based humidity sensor, *Superlattices and Microstructures* **47**, 772-778 (2010).

[64] G. Hu, R. Zhou, R. Yu, L. Dong, C. Pan, and Z. L. Wang, Piezotronic effect enhanced Schottky-contact ZnO micro/nanowire humidity sensor, *Nano Research* **7**, 1083-1091 (2014).

[65] N.H. A. Hardana, A. Jalara, M.A. A. Hamid, L. K. Keng, N.M. Ahmed, and R. Shamsudin, A wide-band UV photodiode based on n-ZnO/p-Si heterojunctions, *Sensors and Actuators A* **207**, 61-66 (2014).

[66] L. C. Chao, C. C. Ye, Y. P. Chen, H. Z. Yu, Facile fabrication of ZnO nanowire-based UV sensors by focused ion beam micromachining and thermal oxidation, *Applied Surface Science* **282**, 384-389 (2013).

[67] A. Ate et al, High performance UV sensor based on individual ZnO nanowire and photoelectric properties of individual ZnO nanowire surface in different atmospheres, *AIP Conf. Proc.* **1586**, 52-56 (2014); doi: 10.1063/1.4866729.

[68] S. Bai, W. Wu, Y. Qin, N. Cui, D. J. Bayer , and X. Wang, High-performance integrated ZnO nanowire UV sensors on rigid and flexible substrates, *Adv. Funct. Mater.* **21**, 4464-4469 (2011).

[69] Z. Alaie, S. M. Nejad, and M. H. Yousefi, Recent advances in ultraviolet photodetectors, *Materials Science in Semiconductor Processing* (2014), DOI: 10.1016/j.mssp.2014.02.054.

[70] A. Menzel, K. Subannajui, F. Güder, D. Moser, O. Paul, and M. Zacharias, Multifunctional ZnO-nanowire-based sensor, *Adv. Funct. Mater.* **21**, 4342-4348 (2011).

[71] F. Xue, L. Zhang, W. Tang, C. Zhang, W. Du, and Z. L. Wang, Piezotronic effect on ZnO nanowire film based temperature sensor, *ACS Appl. Mater. Interfaces* **6** (8), 5955-5961 (2014).

[72] L. Wu, F. F. Song, X. Fang, Z. X. Guo, and S. Liang, A practical vacuum sensor based on a ZnO nanowire array, *Nanotechnology* **21**, 475502 (5pp) (2010).

[73] X. Wang, J. Zhou, J. Song, J. Liu, N. Xu, and Z. L. Wang, Piezoelectric field effect transistor and nanoforce sensor based on a single ZnO nanowire, *Nano Lett.* **6**, 2768-2772 (2006).

[74] Q. Chen, Y. Sun, Y. Wang, H. Cheng, Q. M. Wang, ZnO nanowires–polyimide nanocomposite piezoresistive strain sensor, *Sensors and Actuators A* **190**, 161-167 (2013).

[75] H. Gullapalli, V. S. M. Vemuru, A. Kumar, A. B. Mendez, R. Vajtai, M. Terrones, S. Nagarajaiah, and P. M. Ajayan, Flexible piezoelectric ZnO–paper nanocomposite strain sensor, *Small* **6, No. 15,** 1641-1646 (2010).

[76] N. Kouklin, Cu-Doped ZnO Nanowires for efficient and multispectral photodetection applications, *Adv. Mater.* **20**, 2190-2194 (2008).

[77] Z. Yang, M. Wang, X. Song, G. Yan, Y. Ding, and J. Bai, High-performance ZnO/Ag nanowire/ZnO composite film UV photodetectors with large area and low operating voltage, *J. Mater. Chem. C* **2**, 4312-4319 (2014).

[78] M. H. Mamat, Z. Khusaimi, M. Z. Musa, M. F. Malek, M. Rusop, Fabrication of ultraviolet photoconductive sensor using a novel aluminium-doped zinc oxide nanorod–nanoflake network thin film prepared via ultrasonic-assisted sol–gel and immersion methods, *Sensors and Actuators A* **171**, 241-247 (2011).

[79] C. Jin, S. Park, H. Kim, S. An, and C. Lee, CO gas-sensor based on Pt-functionalized Mg-doped ZnO nanowires, *Bull. Korean Chem. Soc.* **33**, 1993-1997 (2012).

[80] N. Hongsith, C. Viriyaworasakul, P. Mangkorntong, N. Mangkorntong, S. Choopun, Ethanol sensor based on ZnO and Au-doped ZnO nanowires, *Ceramics International* **34**, 823-826 (2008).

[81] D. Y. Kim, and J. Y. Son, Horizontal ZnO nanowires for gas sensor application: Al-doping effect on sensitivity, *Electrochemical and Solid-State Letters*, **12 (12)**, J109-J111 (2009).

[82] X. Chu, S. Zhou, Y. Dong, W. Sun, X. Ge, Trimethylamine gas sensor based on Cr^{3+} doped ZnO nanorods/nanoparticles prepared via solvothermal method, *Materials Chemistry and Physics* **131**, 27-31 (2011).

[83] Q. Wan, Q. H. Li, Y. J. Chen, T. H. Wang, X. L. He, X. G. Gao, and J. P. Li, Positive temperature coefficient resistance and humidity sensing properties of Cd doped ZnO nanowires, *Applied Physics Letters* **84**, 3085-3087 (2004).

[84] Y. Yang, W. Guo, J. Qi, and Y. Zhang, Flexible piezoresistive strain sensor based on single Sb-doped ZnO nanobelts, *Applied Physics Letters* **97**, 223107 (2010).

[85] P. C. Chang, Z. Fan, D. Wang, W. Y. Tseng, W. A. Chiou, J. Hong, and J. G. Lu, ZnO nanowires synthesized by vapor trapping CVD method, *Chem. Mater.* **16**, 5133-5137 (2004).

[86] L. Wang, Y. Pu, Y. F. Chen, C. L. Mo, W. Q. Fang, C. B. Xiong, J. N. Dai, F. Y. Jiang, MOCVD growth of ZnO films on Si(111) substrate using a thin AlN buffer layer, *Journal of Crystal Growth* **284**, 459-463 (2005).

[87] S. Nicolay, S. Fay, and C. Ballif, Growth model of MOCVD polycrystalline ZnO, *Crystal Growth & Design* **9**, 4957-4962 (2009).

[88] R. D. Vispute et al, Heteroepitaxy of ZnO on GaN and its implications for fabrication of hybrid optoelectronic devices, *Applied Physics Letters* **73**, 348-350 (1998).

[89] P. Fons, K. Iwata, S. Niki, A. Yamada, K. Matsubara, Growth of high-quality epitaxial ZnO films on α-Al_2O_3, *Journal of Crystal Growth* **201/202**, 627-632 (1999).

[90] Y. Chen, D. M. Bagnall, H. Koh, K. Park, K. Hiraga, Z. Zhu, and T. Yao, Plasma assisted molecular beam epitaxy of ZnO on c-plane sapphire: Growth and characterization, *Journal of Applied Physics* **84**, 3912-3918 (1998).

Chapter 2: Fundamental properties of ZnO and TM-doped ZnO

ZnO is a II–VI semiconductor material and it is a very promising material for semiconductor device applications due to its wide range of useful properties. ZnO has a direct wide band gap of 3.44 eV at low temperatures and 3.37 eV at room temperature, which enables some applications in optoelectronics such as light-emitting diodes, laser diodes and photodetectors, it has relatively large exciton binding energy (60 meV), which makes ZnO a promising material for excitonic effects based optical devices and due to the lack of a center of symmetry in wurtzite structure combined with a large electromechanical coupling, ZnO possesses large piezoelectric and pyroelectric properties. These makes the ZnO generally used for sensors, transducers and actuators. In addition, ZnO is a biocompatible and biosafe and ZnO is also phototoxic intracellular, which attracts ZnO for chemical sensor and biosensors applications [1-5]. Moreover, transition metals (TM)-doped ZnO can be change its properties. This is due to the fact that TM-doped ZnO have intrinsic donor defects which contributes to carrier and optical property and it enhanced ferromagnetic properties at room temperature, which makes TM-doped ZnO useful for spintronic applications [1, 3, 6-11]. Furthermore, ZnO possesses diverse nanostructures, such as nanotubes, nanowires, nanorods, nanobelts, nanotetrapods, nanoribbons, nanorings, nanocombs, and so on and these ZnO nanostructures can possibly be grown on cheap and flexible substrates. Hence, ZnO nanostructures are attractive and promising material for some future nanotechnology applications [12-14]. However, most of these advantages are definitely utilized due to the fundamental properties of ZnO nanomaterial. Therefore, the basic properties of ZnO and TM-doped ZnO nanostructures will be introduced in this chapter.

2.1 Crystal structure and chemical binding

ZnO is one of the II-VI compound semiconductors whose ionicity resides in between being covalent and ionic semiconductor. The crystal structures of ZnO are wurtzite (*B4*), zinc blende (*B*3), and rocksalt (*B1*). However under ambient conditions, the thermodynamically stable phase is the wurtzite [3, 15]. ZnO crystallizes usually in the hexagonal wurtzite-type structure shown in Figure 2.1. In this phase, the ZnO has a polar hexagonal axis called the *c-axis* that is parallel to the *z-axis*. The primitive translation vectors ***a*** and ***b*** with equal length lay in the *x-y* plane which makes an angle of 120° and the primitive translation vector ***c*** is parallel to the *z-axis* [16]. At room temperature, the wurtzite structure has a hexagonal unit cell with lattice parameters a = b ≈ 0.3249 nm and c ≈ 0.5206 nm and the ratio c/a value is around 1.602,

which is slightly different from the ideal value c/a = 1.633 for hexagonal structure. The point group is 6 mm or C_{6v} and the space group is $P6_3mc$ in Hermann–Mauguin notation and C_{6V}^4 in Schoenflies notation [15-17]. Every atom of one kind (group II atom) is surrounded by four atoms of the other kind (group VI), or vice versa, which means that one zinc ion (cation) is surrounded tetrahedrally by four oxygen ions (anions) and vice versa. Its structure is arranged by alternating planes of tetrahedrally coordinated O^{2-} and Zn^{2+} ions stacking along the *c-axis*, which makes the entire structure to lack central symmetry. The surfaces can be terminated either with cations or anions, which leads ZnO possesses positively or negatively charged on the surfaces [18].

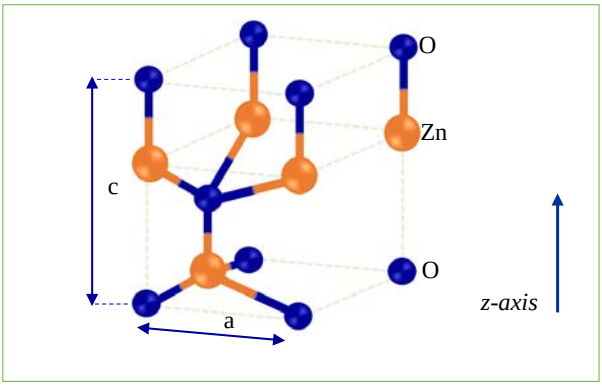

Figure 2. 1: *The hexagonal wurtzite of ZnO crystal structure (adopted from [3, 15-17]).*

2.2 Basic physical parameter for Wurtzite ZnO

As mention earlier, nanotechnology applications are partly relying on the fundamental properties of the nanomaterial. Therefore, understanding the fundamental physical properties of ZnO is important to the rational design of functional devices. It should be noted that as the dimension of the semiconductor materials shrink down to nanometer scale, some of their physical properties undergo changes due to "quantum size effects". However, some of these parameters of ZnO are not well demonstrated, e.g. hole mobility and effective mass are still under debate. Table 2.1 shows some of the basic physical parameters for wurtzite ZnO [19-22]. However, investigation of the properties of individual ZnO nanostructures is essential for developing their nanoscale devices.

Table 2. 1: *Some basic physical parameters for wurtzite ZnO.*

Physical parameters		**Value**
Lattice parameters at 300 K	a_0	0.324 95 nm
	c_0	0.520 69 nm

	a_0/c_0	1.602 (ideal hexagonal structure 1.633)
	u	0.345
Density		5.606 g/cm^3
Stable phase at 300 K		Wurtzite
Melting point		2248 K
Linear expansion coefficient (/°C)		a_0: 6.5×10^{-6}
		c_0:3.9 x 10^{-6}
Static dielectric constant		8.656
Refractive index		2.008, 2.029
Energy gap (300 K)		3.37 eV (direct band gap)
Intrinsic carrier concentration		<10^6 cm^{-3} (max n-type doping>10^{20} cm^{-3} electrons; max p-type doping<10^{17} cm^{-3} holes)
Exciton binding energy		60 meV
Ionicity		62%
Electron effective mass		0.24
Electron mobility (T = 300 K)		200 cm^2/V·s
Hole effective mass		0.59
Hole mobility (T = 300 K)		5-50 cm^2/V·s

2.3 Band structure of Wurtzite ZnO

The band structure is a very important property of a semiconductor, because many important properties and parameters are derived from it, e.g. band gap and effective masses of electrons and holes. For this reason, understanding of the band structure of ZnO is crucial to explain the electrical properties, optical properties and many other phenomena. The band structure provides the electronic one-particle (i.e. electron or hole) states. ZnO is a direct band gap semiconductor which crystallizes in the wurtzite symmetry because the uppermost valence band (VB) and the lowest conduction band (CB) are at the same position in the Brillouin zone, namely at **k**=0, i.e. at the Γ-point [16-17]. The lowest CB is formed from the empty 4s states of Zn^{2+} or the anti-binding sp^3 hybrid states and the VB originates from the occupied 2p orbitals of O^{2-} or the binding sp^3 orbitals. Under the crystal field and spin orbit interaction, the valence band is split into three sub-VB of symmetries, which are labelled in all wurtzite-type semiconductors from high to low energies as A, B, and C bands. In most cases, the ordering of the bands is A Γ_9, B Γ_7, C Γ_7. However, for ZnO there is a long debate whether the ordering as

usual or A Γ_7, B Γ_9, C Γ_7. Therefore, the ordering A Γ_7, B Γ_9, C Γ_7 have been selected [16-17, 23] (see Figure 2.2). The relation between the band gap and temperature dependence up to 300 K is given by:

$$E_g(T) = E_g(T=0)\frac{5.05 \times 10^{-4} \times T^2}{(900 - T)} \tag{2.1}$$

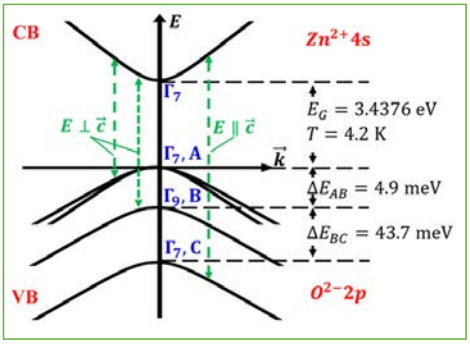

Figure 2. 2: *The valence band (VB) and conduction band (CB) of ZnO in the vicinity of the fundamental band-gap. (adopted from [16-17 and 23]).*

2.4 Electrical properties

Un-doped ZnO semiconductor often shows n-type conductivity due to its native defects such as oxygen vacancies and zinc interstitials [22]. As mention earlier, ZnO semiconductor material is a direct and wide band gap material with a relatively large exciton binding energy, which is attractive for many electronic and optoelectronic applications. This is because of wide band gap materials may have high breakdown voltages, lower noise generation, ability to sustain large electric fields, and it can operate at high temperature with high power. The electron transport in ZnO is different at sufficiently low and high electric fields [3, 15]. When a low electric field is applied, the energy gained by the electrons from the field is small as compared to the thermal energy of electrons. Hence, the energy distribution of electrons in the ZnO is unaffected by applying low electric field. Therefore, the electron mobility remains constant because the scattering rate, which indicates that the electron mobility remains independent of applied low electric fields, and Ohm's law is obeyed [3, 15]. When the electrical field is increased to a point that the energy of electrons from the applied electrical field is no longer negligible compared to the thermal energy of the electron, then the electron distribution function changes significantly from its equilibrium value and these electrons become hot electrons with higher temperature than the lattice temperature. Therefore, there is no energy

dissipated to the lattice during a short and critical time and when the drift velocity of an electron is higher than its steady-state value, a higher frequency device is possible to fabricate [3, 15].

2.5 Piezoelectric properties

The mechanical properties of materials involve various concepts, including piezoelectric constants. The physical quantity called ***strain*** is described as the deformation of solids under the effect of external forces and the physical quantity called ***stress*** is described as the internal mechanical force that resists deformation and tends to return the solid to its initial state [15]. Piezoelectric properties is due to the polarization at atomic level. The mechanical strain can affect the charge carrier transport in materials. For a homogeneous material, three mechanisms may alter its transport characteristics, including the geometric change, the piezoresistive effect (changes the material resistivity), and the piezotronic effect [24]. In case of wurtzite ZnO nanostructures, the origin of the piezoelectricity is described as the following: consider an atom with a negative charge that is surrounded tetrahedrally by positive charges, in which the oxygen atoms and zinc atoms are tetrahedrally bonded. When an external force is exerted on the crystal along the direction of the tetrahedron, the center of the positive charge and the negative charge can be displaced due to lattice distortion. This distortion can cause the center of positive charge and negative charge to displace from each other, which induces local dipole moments. If the whole crystals have the same orientation, the crystals will possess macroscopic dipole moments, while it is experiencing the external force or external pressure [13, 21-22]. The ZnO nanostructure comprises alternating layers of Zn^{+2} and O^{-2} atoms stacking along the *c-axis* with a lack of center of symmetry in ZnO, leading ZnO to possesses a strong piezoelectricity property providing a relatively large electromechanical coupling. This offers significant potential for applications in nano-electromechanical systems, sensor development and electromechanically coupled sensors and transducers [16, 20-21].

2.6 Optical properties

The optical properties of a semiconductor are related to its intrinsic and extrinsic factors. Intrinsic optical properties related to the relation between electrons in the conduction band (CB) and holes in the valence band (VB), including excitonic effects due to the Coulomb interaction. Extrinsic properties are related to dopants or defects introduced in the semiconductor, which generate discrete electronic states between CB and VB [3]. Optical transitions in ZnO have been investigated by various experimental techniques such as optical absorption, transmission, reflection, photoluminescence, cathodoluminescence, etc. Among

these techniques, the photoluminescence (PL) technique have been extensively used to study the optical properties of ZnO nanostructures. Typically, room temperature PL spectrum of ZnO shows UV emission and one or two visible emissions induced by defects, including vacancies (missing atoms at regular lattice positions), interstitials (extra atoms occupying interstices in the lattice), antisites (a Zn atom occupying an O lattice site or vice versa) and complex defects [2, 12]. At room temperature, ZnO exhibits a wide and direct band-gap of 3.37 eV with a relatively large exciton energy of 60 meV. The value of 60 meV is much larger than that of GaN (25 meV), and the thermal energy at room temperature (26 meV), which ensures that an efficient exciton emission at room temperature under low excitation energy. Therefore, ZnO is one of the promising photonic material in the blue-UV region [13]. For ZnO nanorods, photoluminescence spectroscopy has been widely used to investigate the optical properties, which provides information such as band gap, defects, and crystal quality [13, 22]. Room temperature PL investigation of ZnO nanorods shown that a near band edge (NBE) UV emission and a broader band emission related to deep level defects, i.e. deep level emission (DLE) have been observed in ZnO nanorods and there is only one emission centered at UV emission (varies in a range from 3.236 to 3.307 eV) have been observed in high quality ZnO nanorods with low impurity concentrations [1]. The UV emission attributed to the NBE emission of the wide band gap ZnO and the DLE bands within the visible range are attributed to defects in the ZnO nanostructure such as Oxygen vacancy (V_O), Zinc vacancy (V_{Zn}), Oxygen interstitial (O_i), Zinc interstitial (Zn_i) and extrinsic impurities [1, 13]. The relative intensity between the NBE emission and DLE emission can be used as an indication of the optical quality of the ZnO nanostructures. Therefore, the optical quality of the ZnO nanostructures can be investigated by the ratio of the intensity of the near band edge emission to the intensity of the deep level emission (I_{NBE}/I_{DLE}). A large ratio of the I_{NBE}/I_{DLE} means a lower concentration of the deep level defect [1].

2.7 Characteristics of TM-doped-ZnO

2.7.1 Brief theory for ferromagnetic properties in DMS

Dilute magnetic properties of transition metal doped semiconductors, called diluted magnetic semiconductors (DMS), provide an alternative way to make the semiconductors ferromagnetic at room temperature. The DMSs are used for potential applications in spin-transport electronics (spintronics) devices, which exploit spin in magnetic materials along with charge of the electrons in a DMS material. The synthesis of ferromagnetic semiconductors that works at room temperature remains very attractive for device applications [3]. The *3d* TM ions

such as Sc, Ti, V, Cr, Mn, Fe, Co, Ni, and Cu have partially filled *d* shells are substituted for the cations of the host semiconductors, which leads to achieve the DMS.

The magnetic property of a DMS is found to be a strong function of the TM ions concentration in the crystal, the carrier density, and the crystal quality [10]. The electronic structure of the substituted TM in semiconductors is influenced by two factors, i.e. strong 3d-host hybridization and strong Coulomb interactions between 3d-3d electrons [25]. The reason for providing magnetic property at higher temperatures is due to the quantum mechanical exchange interaction between two electrons. In general, when all the atomic magnetic moments in the lattices interact to align parallel (↑↑) to each other, the material exhibits ferromagnetism with nonzero magnetic moment even in the absence of an external magnetic field, called the spontaneous magnetic moment. This phenomenon is called ferromagnetism and the magnetic moments are aligned parallel. The observed transition temperature below the ferromagnetic ordering is called Curie-temperature T_C [10, 25]. However, if the adjacent of the magnetic moments are oriented anti-parallel. i.e. compensates one another, the semiconductor material is antiferromagnetic and there is no spontaneous magnetization can observed, even in the external magnetic field [11, 26]. The magnetic ordering being ferromagnetic (↑↑) or antiferromagnetic (↑↓) of semiconductor is shown in Figure 2.3.

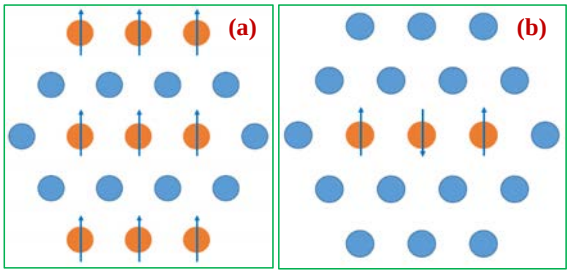

Figure 2. 3: *(a) Ferromagnetic DMS, an alloy between nonmagnetic semiconductor and TM and (b) antiferromagnetic DMS. (adopted from [11, 26])*

2.7.2 Brief theory of ZnO-based magnetic semiconductors

Generally, the portion of TM atoms randomly incorporated in the semiconductors provide localized magnetic moments in the DMS matrix [9]. The electronic configuration of the *3d* states and *4s* states of several TM are shown in Figure 2.4. For Mn ions, among the 10 available states of 3*d* band of Mn^{2+} ions, half-filled with 5 electrons with an energy gap between the up-spin (↑) occupied states and empty down-spin (↓) states and for the 3*d* band. For Fe or Co, one of the bands is partially filled (up or down). Table 2.2 presents the oxidation and charge states for Mn and Fe presented in ZnO [25].

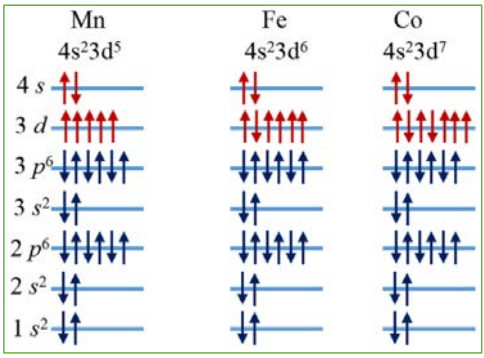

Figure 2. 4: *Electronic configuration of 3d-states and 4s-states of TMs [9, 25].*

Wurtzite ZnO is formed by tetrahedral (s-p^3) bonding between zinc and oxygen. When TM ions such as Mn ions are substituted in the ZnO matrix (replacing the Zn sites), the TM ions contribute their $4s^2$ electrons to the s-p^3 bonding and form a TM^{2+} charge state. The TM-*d* bands hybridize with the O-*p* bands in the ZnO matrix and form the tetrahedral bonding in the ZnO based DMS, which exchanges the interaction between the localized 3*d* spins and carriers in the host valence band [9].

Currently, the theoretical studies of ferromagnetism in DMS based ZnO is under debate. However, the most suitable model for studying the nature and the origin of ferromagnetism in the system of the n-type ZnO doped with TM is called spin-split-orbit model [6, 27]. In this model, the longer ferromagnetic exchange can be mediated by shallow donor electrons of bound magnetic polarons formed by point defects like oxygen vacancies [28-29]. If the nearby TM ions possess parallel magnetic moments, the *3d* electrons in TM *d* band are allowed to hop to the *3d* orbitals of the neighboring TM, which is mediated by charge carriers in a spin-split impurity band formed by the donor states, therefore, the shallow donor levels get hybridized with the TM *d* band and stabilize the ferromagnetic ground state in the system [6, 27].

In this model, the high T_C occurred only when the *3d* states of the TM hybridizes with spin-split-impurity-band states lie at the Fermi level [28-29].

Table 2. 2: *Expected oxidation and charge state of Mn and Fe ions presented in ZnO. Neutral state is referred as the same charge state as Zn ions in the ZnO [9, 25].*

ZnO	**3*d*^{3}**	**3*d*^{4}**	**3*d*^{5}**	**3*d*^{6}**
Acceptor [(-)charge]				Mn^{+}
Neutral			Mn^{2+}	Fe^{2+}
Donor [(+) charge]		Mn^{3+}	Fe^{3+}	
Double donor [(2^{+} charge)]	Mn^{4+}	Fe^{4+}		

References

[1] M. Willander et al, Zinc oxide nanorod based photonic devices: recent progress in growth, light emitting diodes and lasers, *Nanotechnology* **20**, 332001(40page) (2009).

[2] A. Janotti and C. G. Van de Walle, Fundamentals of zinc oxide as a semiconductor, *Rep. Prog. Phys.* **72**, 126501 (29pages) (2009).

[3] Ü. Özgür, Ya. I. Alivov, C. Liu, A. Teke, M. A. Reshchikov, S. Doan, V. Avrutin, S. J. Cho, and H. Morkoç, A comprehensive review of ZnO materials and devices, *Journal of Applied Physics* **98**, 041301 (2005).

[4] Z. L. Wang, and J. Song, Piezoelectric nanogenerators based on zinc oxide nanowire arrays, *Science*, Vol.**312, No. 5771**, 242-246 (2006).

[5] Z. L. Wang, and W. Wu, Piezotronics and piezo-phototronics: fundamentals and applications, *National Science Review* **1**, 62-90 (2014).

[6] S. J. Pearton, D. P. Norton, M. P. Ivill, A. F. Hebard, J. M. Zavada, W. M. Chen, and I. A. Buyanova, ZnO doped with transition metal ions, *IEEE Transactions on electron Devices*, **Vol. 54, No. 5**, 1040-1048 (2007).

[7] I. A. Buyanova, W. M. Chen, M. P. Ivill, R. Pate, D. P. Norton, S. J. Pearton, J. W. Dong, A. Osinsky, B. Hertog, A. M. Dabiran, and P. P. Chow, Optical characterization of ZnMnO-based dilute magnetic semiconductor structures, *Journal of Vacuum Science & Technology B* **24**, 259-262 (2006).

[8] A. Gorzkowska-Sobas, A. Galeckas, M. F. Sunding, S. Diplas, and A. Yu. Kuznetsov, An investigation of Fe-doped ZnO thin films grown by magnetron sputtering, *Phys. Scr.* **T141**, 014004 (7pp) (2010).

[9] C. Liu, F. Yun, H. Morkoc, Ferromagnetism of ZnO and GaN: A review, *Journal of Materials Science: Materials in Electronics* **16**, 555-597 (2005).

[10] S. J. Pearton, D. P. Norton, M. P. Ivill, A. F. Hebard, J. M. Zavada, W. M. Chen, and I. A. Bunyanova, Ferromagnetism in transition-metal doped ZnO, *Journal of Electronic Materials* **36**, No. 4, 462-471 (2007).

[11] T. Dietl, Dilute magnetic semiconductors: Functional ferromagnets, *Nature Materials* **2**, 646-648 (2003).

[12] A. B. Djurisic, and Y. H. Leung, Optical properties of ZnO nanostructures, *Small* **2**, **No. 8-9**, 944-961 (2006).

[13] Z. L. Wang, Zinc oxide nanostructures: growth, properties and applications, *J. Phys.: Condens. Matter* **16**, R829-R858 (2004).

[14] A. K. Radzimska, and T. Jesionowski, Zinc oxide—from synthesis to application: A review, *Materials* **7**, 2833-2881 (2014).

[15] H. Morkoc and U. Ozgur, General properties of ZnO, Zinc Oxide: Fundamentals, materials and device technology, *WILEY-VCH Verlag* (2009) p.1-2.

[16] C. Klingshirn, ZnO: From basics towards applications, *Phys. Stat. Sol. (b)* **244** No. 9, 3027-3073 (2007).

[17] C. Klingshirn, ZnO: Material, physics and applications, *ChemPhysChem* **8**, 782-803 (2007).

[18] Z. L. Wang, ZnO nanowire and nanobelt platform for nanotechnology, *Materials Science and Engineering* **R 64**, 33-71 (2009).

[19] S.J. Pearton, D.P. Norton, K. Ip, Y.W. Heo, T. Steiner, Recent progress in processing and properties of ZnO, *Progress in Materials Science* **50**, 293-340 (2005).

[20] S. Singh et al, Structure, microstructure and physical properties of ZnO based materials in various forms: bulk, thin film and nano, *J. Phys. D: Appl. Phys.* **40**, 6312-6327 (2007).

[21] Z. Fan and J. G. Lu, Zinc Oxide Nanostructures: Synthesis and properties, *J. Nanosci Nanotechnol.* **5**, 1561-73 (2005).

[22] J. Cui, Zinc oxide nanowires, *Materials Characterization* **64**, 43-52 (2012).

[23] B. K. Meyer et al, Bound exciton and donor–acceptor pair recombinations in ZnO, *Phys. Stat. Sol. (b)* **241**, No. 2, 231-260 (2004).

[24] R. Zhu and R. Yang, Separation of the piezotronic and piezoresistive effects in a zinc oxide nanowire, *Nanotechnology* **25**, 345702 (6pp) (2014).

[25] H. Morkoç and U. Özgur, Zinc Oxide: Fundamentals, materials and device technology, *WILEY-VCH Verlag GmbH & Co. KGaA*, Weinheim (2009) p.284-287.

[26] H. Ohno, Making nonmagnetic semiconductors ferromagnetic, *Science* **281**, 951-956 (1998).

[27] D. Karmakar, S. K. Mandal, R. M. Kadam, P. L. Paulose, A. K. Rajarajan, T. K. Nath, A. K. Das, I. Dasgupta, and G. P. Das, Ferromagnetism in Fe-doped ZnO nanocrystals: Experiment and theory, *Physical Review B* **75**, 144404 (2007).

[28] J. M. D. Coey, M. Venkatesan and C. B. Fitzgerald, Donor impurity band exchange in dilute ferromagnetic oxides, *Nature Materials* **4**, 173-179 (2005).

[29] M. Venkatesan, C. B. Fitzgerald, J. G. Lunney, and J. M. D. Coey, Anisotropic ferromagnetism in substituted zinc oxide, *Physical Review Letters* **93**, No. 17, 177206 (4 pages) (2004).

Chapter 3: Sensors and their applications based on ZnO nanorods

As we have mentioned in the chapter 1, a sensor is a device that sense to a change of physical conditions/chemical/biological quantities which produces a measurable signal. Due to the quantum confinement effects in semiconductor nanostructures with the ability to tailor the size, structure and properties, therefore, the construction of sensors based nanomaterials offers excellent prospects for designing novel sensing systems, which provides sensors based nanomaterials of high sensitivity, improved detection limits, faster responses, smaller amounts of samples can be measurable, lower cost, easy to use for un-skills users, high-efficiency and less power consumption. Among metal oxide nanomaterials, zinc oxide (ZnO) nanostructures is one of the most promising metal oxides due to their attractive physical and chemical properties. Especially, 1-D ZnO nanostructures such as nanorods, nanowires, nanobelts, and nanotube, are becoming a major focus in nanoscience research and are of interest for many different applications due to their important physical properties and application prospects. Therefore, the background of sensors, including biosensors, piezoresistive sensor, and UV photodetector and the applications of ZnO nanorods based sensors is provided in the following sections.

3.1 Biosensors and their applications based on ZnO nanorods

The concept of biosensors started from 1956 by L. C. Clark which is known as the founder of the oxygen electrode sensor [1]. In 1962 Clark developed a first biosensor by immobilizing enzyme glucose oxidase on the modified oxygen electrodes and utilized as an electrochemical detector. The amount of glucose in the solution can measured by the consumption of the dissolved oxygen [2]. In 1967, the immobilized enzyme glucose oxidase electrode was developed to measure the concentration of glucose in the biological solution and in the tissues in vitro [3]. A biosensor uses a biomaterial to sense to the target analytes and converts a biological response into a measureable signal. It consist of two parts called bio-receptor (biological recognition element) such as enzyme, antibody, aptamer, and microorganism, which selectively recognizes the target analytes, and transducer, which converts biological response to a measurable signal such as current, voltage, resistance, capacitance, mass, light intensity, … etc. Currently, biosensors have been used in many applications such as medicine, medical diagnosis, biomedical research, drug delivery, environmental monitoring, food content, quality and safety, security and defence [4-13].

The most importance of biosensors is related to high sensitivity, selectivity, chemical stability, biocompatibility, minimum hardware requirements, fast response time, low cost, and comfortable for unskilled users. Therefore, the transducer made from the nanomaterials that possess excellence electrical, optical, magnetic, and mechanical properties is high requirement. Among the biosensors, electrochemical biosensors have been the most widely used in biosensing applications. The transducers sense to a biochemical signal produced by a bio-receptor via an amperometric, potentiometric or conductometric pathway. Furthermore, electrochemical devices are uniquely qualified for small size, low cost, low volume, minimum hardware requirements, and power requirements of decentralized testing and indicate great promise for a wide range of biomedical or environmental applications [11-12]. In electrochemical biosensors, electron transfer between redox-active biomolecules to electrodes does not always occur directly but it occurs through the use of redox mediators. However, in biosensors based on direct electron transfer (DET), the absence of mediators provides the biosensors with high selectivity because both the electrode material and the enzyme operate in a potential window closer to the redox potential of the enzyme itself, which makes biosensors resist to interfering reactions [11]. The electrochemical transducer based metal oxides nanostructures promote the direct electron transfer reactions, amplification and orient the analytic signal of the bio-recognition response without addition of a mediator to the analyzed solution. The metal oxides based transducers are suitable for direct and fast biosensors, which can directly convert the biological recognition response to electrical signal [13]. In particular, 1-D ZnO nanostructures possess many remarkable properties for biosensors applications due to their high catalytic efficiency, high surface area to volume ratio, biocompatibility, chemical stability and strong adsorption ability because of the high isoelectric point (IEP ~ 9.5), and high ionic characteristics (60%), not dissolve at biological pH and fast electron transfer. Moreover, the advantages of using ZnO nanorods for sensing applications have gained much attraction due to their high surface area to volume ratio which makes biosensors extremely sensitive to minute surface changes, time domain chemical sensing for low concentrations and the possibility of sensing in single cells or molecule detection available in small volumes at low concentration [14-17]. These properties make ZnO nanorods ideal candidates for biosensor applications, which cannot be achieved simultaneously using large sized sensors.

3.2 Piezoresistive sensor and its applications based on ZnO nanorods

The piezoresistive effect describes the changes of electrical resistance in certain semiconductor materials by applying external force or material deformation [18-19]. This effect provides direct relation between external mechanical energy and electrical signal. The piezoresistive effect is widely utilized as a low energy piezoelectronic switch [20], accelerometers, pressure/force sensors, gyro-rotation rate sensors, flow sensors, tactile sensors, sensors for monitoring structural integrity of mechanical elements, and for chemical/biological sensors [21]. It noted that, silicon piezoresistive effect is widely used, today. In general, piezoresistive devices are utilizing different materials like graphene [22-23], carbon nanotube [24-26], rare-earth chalcogenide enabling nanomechanical switching [27], ZnO nanowires–polyimide nanocomposite [28], Sb-doped ZnO nanobelts [29], and ZnO porous films [30]. A typical piezoresistive sensor consists of a semiconductor and two metal electrodes on the ends, either both electrodes are Ohmic contacts or one electrode is Ohmic and other electrode is Schottky contacts. The change of current transport characteristics under different applied forces at two contacts are measures. Generally, either Schottky contact or Ohmic contact on a ZnO nanorods is solely determined by their work functions. In particular for piezoresistive sensor based on ZnO nanorods, a large area of the samples with homogenous morphological properties i.e. uniform size distribution and high degree of alignment, are all required in order to obtain a linear reproducible response from a piezoresistive sensor. In particular and considering the piezoelectric property, well-aligned ZnO nanorods play an important role in achieving an improved performance [31]. The method to synthesize the well-aligned with uniform size distribution of ZnO nanorods and the selected Ohmic and Schottky contacts for fabrication of piezoresistive sensor applications will discuss in chapter 4.

3.3 UV photodetector and its applications based on ZnO nanorods

Ultraviolet (UV) photodetector is a UV light-sensitive devices used to detect UV radiation through electronic processes. In general, the principle operating of all solid-state photosensitive devices involve three steps, carrier generation by absorption of the incident light, carriers transport in the device and interaction of current with the external circuit to provide measurable output signal [32]. Recently, UV photodetector has a large range applications such missile launching detection, flame sensing, UV-radiation calibration and monitoring, engine control, chemical and biological analysis, solar UV monitoring, lithography aligners, optical communications and astronomy [32-

36]. The responsivity and response time are the main characteristics to describe the performance of the UV photodetector. The UV photodetector possesses higher responsivity and fast response time are required for the above applications. Recently, several wide direct band gap semiconductor materials are under intensive investigates in order to improve the responsivity and stability of UV photodetector. Among them, ZnO nanostructures is one of the most important wide direct band gap (3.37eV) and high exciton binding energy (60 meV) at room temperature, which makes ZnO nanostructures is very promising semiconductor nanomaterial for the UV photodetector [33-36]. In addition, ZnO nanorods possess large surface area to volume ratio, which provided the oxygen adsorption and desorption at the surfaces of ZnO nanorods [33]. Moreover, the performance of sensors can be improve by doping ZnO nanostructures with different metals. This is due to the fact that metal-doped ZnO nanostructures have intrinsic donor defects which contributes to carriers and optical properties, which generates more electron-hole pairs under UV excitation. Due to there are several challenges for obtaining reliable p-type ZnO which limits to make homojunction p–n junction based ZnO devices, therefore, metal-ZnO-metal structures based UV photodetectors are of interest to researchers. Schottky diode based UV photodetectors are more attractive since it provides high gain, high speed and low noise performance, while Ohmic junction based photodetector has very long decay time and large dark current [33]. Therefore, Schottky diode based on ZnO and metal-doped ZnO nanorods are potential candidate for high performance UV photodetectors and low-cost, large-scale mode of flexible electronics also can be achieved by low temperature hydrothermal synthesis.

References

[1] L. C. Clark Jr., Monitor and control of blood and tissue oxygen tensions, *Transactions of the American Society for Artificial Internal Organs* **2**, 41-48 (1956).

[2] L. C. Clark Jr., and C. Lyons, Electrode systems for continuous monitoring in cardiovascular surgery, *Annals New **York** Academy of Sciences* **102**, 29-45 (1962).

[3] S. J. Updike, and J. P. Hicks, The enzyme electrode, *Nature* **214**, 986-988 (1967).

[4] S. Rodriguez-Mozaz, M. J. Lopez de Alda, D. Barceló, Biosensors as useful tools for environmental analysis and monitoring, *Anal Bioanal Chem* **386**, 1025-1041 (2006).

[5] S. Rodriguez-Mozaz, M. J. Lopez de Alda, M. P. Marco, D. Barcelo, Biosensors for environmental monitoring: A global perspective, *Talanta* **65**, 291-297 (2005).

[6] S. Rodriguez-Mozaz, M. P. Marco, M. J. Lopez de Alda, and D. Barceló, Biosensors for environmental applications: Future development trends, *Pure Appl. Chem.* **76** No. 4, 723-752 (2004).

[7] S. Su, W. Wu, J. Gao, J. Lu, and C. Fan, Nanomaterials-based sensors for applications in environmental monitoring, *J. Mater. Chem.* **22**, 18101-18110 (2012).

[8] S. Wang, X. Zhu, and M. Zhao, Chapter 2: Optical sensors based on molecularly imprinted nanomaterials, Smart nanomaterials for sensor application, *Bentham Science Publishers* (2012) 60-73.

[9] P. R. Solanki, A. Kaushik, V. V. Agrawal, and B. D. Malhotra, Nanostructured metal oxide-based biosensors, *NPG Asia Mater*. **3(1)**, 17-24 (2011).

[10] N. S. Ramgir, Y. Yang, and M. Zacharias, Nanowire-based sensors, *small* **6**, 1705-1722 (2010).

[11] S. K. Arya, S. Saha, J. E. Ramirez-Vick, V. Gupta, S. Bhansali, S. P. Singh, Recent advances in ZnO nanostructures and thin films for biosensor applications: Review, *Analytica Chimica Acta* **737**, 1-21 (2012).

[12] J. Wang, Nanomaterial-based electrochemical biosensors, *Analyst* **130**, 421-426 (2005).

[13] A. A. Ansari, M. Alhoshan, M. S. Alsalhi, and A. S. Aldwayyan, Chapter 2: Nanostructured metal oxides based enzymatic electrochemical biosensors, Book: Biosensors, InTech (2010) 23-46. DOI: 10.5772/45616

[14] M. M. Rahman, A. J. Saleh Ahammad, J. H. Jin, S. J. Ahn, and J. J. Lee, A Comprehensive review of glucose biosensors based on nanostructured metal-oxides, *Sensors* **10**, 4855-4886 (2010).

[15] Z. H. Ibupoto, S. M. Usman Ali, K. Khun, C. O. Chey, O. Nur and M. Willander, ZnO nanorods based enzymatic biosensor for selective determination of Penicillin, *Biosensors* **1**, 153-163 (2011).

[16] M. Willander and O. Nur, Applications of zinc oxide nanowires for biophotonics and bio-electronics, DOI: 10.1117/2.1201101.003498.

[17] M. Q. Israr, J. R. Sadaf, M. H. Asif, O. Nur, M. Willander, and B. Danielsson, Potentiometric cholesterol biosensor based on ZnO nanorods chemically grown on Ag wire, *Thin Solid Films* **519**, 1106-1109 (2010).

[18] S. Stassi, V. Cauda, G. Canavese, and C. F. Pirri, Flexible tactile sensing based on piezoresistive composites: A review, *Sensors* **14**, 5296-5332 (2014).

[19] M. Melnykowycz, B. Koll, D. Scharf, and F. Clemens, Comparison of piezoresistive monofilament polymer sensors, *Sensors* **14**, 1278-1294 (2014).

[20] P.M. Solomon et al, "The piezoelectronic switch: A path to low energy electronics", energy efficient electronic systems (E3S), Third Berkeley Symposium, *IEEE* (2013) 28-29. DOI: 10.1109/E3S.2013.6705880.

[21] C. Liu, Piezoresistive sensors, in: Foundations of MEMS (2nd Edition), *Prentice Hall*, Upper Saddle River, 2012, pp.207.

[22] C. Yan, J. Wang, W. Kang, M. Cui, X. Wang, C. Y. Foo, K. J. Chee, and P. S. Lee, Highly Stretchable Piezoresistive Graphene–Nanocellulose Nanopaper for Strain Sensors, *Adv. Mater.* **26**, 2022-2027 (2014).

[23] H. B. Yao, J. Ge, C. F. Wang , X. Wang, W. Hu, Z. J. Zheng, Y. Ni , and S. H. Yu, A flexible and highly pressure-sensitive graphene–polyurethane sponge based on fractured microstructure design, *Adv. Mater.* **25**, 6692-6698 (2013).

[24] O. Kanoun et al, Flexible carbon nanotube films for high performance strain sensors, *Sensors* **14**, 10042-10071 (2014).

[25] A. Bsoul, M. S. Mohamed Ali, A. Nojeh, and K. Takahata, Piezoresistive strain sensing using carbon nanotube forests suspended by Parylene-C membranes, *Appl. Phys. Lett.* **100**, 213510 (2012).

[26] D. Thuau, C. Ayela, P. Poulin, I. Dufour, Highly piezoresistive hybrid MEMS sensors, *Sensors and Actuators A* **209**, 161-168 (2014).

[27] M. Copel, Giant piezoresistive on/off ratios in rare-earth chalcogenide thin films enabling nanomechanical switching, *Nano Lett.***13**, 4650-4653 (2013).

[28] Q. Chen, Y. Sun, Y. Wang, H. Cheng, Q. M. Wang, ZnO nanowires–polyimide nanocomposite piezoresistive strain sensor, *Sensors and Actuators A* **190**, 161-167 (2013).

[29] Y. Yang, W. Guo, J. Qi, and Y. Zhang, Flexible piezoresistive strain sensor based on single Sb-doped ZnO nanobelts, *Applied Physics Letters* **97**, 223107 (2010).

[30] Q. Zeng, D. Lei, Y. Zhang, and H. Huang, Transferable self-supporting ZnO porous films for low-cost piezoresistive sensors, *Semicond. Sci. Technol.* **29**, 045009 (5pp) (2014).

[31] Z. L. Wang, ZnO nanowire and nanobelt platform for nanotechnology, *Materials Science and Engineering* **R 64**, 33-71 (2009).

[32] L. Luo, Y. Zhang, S. S. Mao, L. Lin, Fabrication and characterization of ZnO nanowires based UV photodiodes, *Sensors and Actuators A* **127**, 201-206 (2006).

[33] Z. Alaie, S. M. Nejad, M. H. Yousefi, Recent advances in ultraviolet photodetectors, *Materials Science in Semiconductor Processing*, DOI: 10.1016/j.mssp.2014.02.054.

[34] P. Sharma, K. Sreenivas, and K. V. Rao, Analysis of ultraviolet photoconductivity in ZnO films prepared by unbalanced magnetron sputtering, *Journal of Applied Physics* **93**, 3963-3770 (2003).

[35] C. Periasamy and P. Chakrabarti, Large-area and nanoscale n-ZnO/p-Si heterojunction photodetectors, *Journal of Vacuum Science & Technology B* **29**, 051206 (2011).

[36] N. H. Al-Hardan, A. Jalar, M. A. Abdul Hamid, L. K. Keng, N. M. Ahmed, R. Shamsudin, A wide-band UV photodiode based on n-ZnO/p-Si heterojunctions, *Sensors and Actuators A* **207**, 61-66 (2014).

Chapter 4: Experimental methods

4.1 Synthesis of ZnO and TM-doped ZnO nanorods

As mentioned in the chapter 2, ZnO is a multifunctional material and its diverse nanostructures can possibly be grown on any cheap and flexible substrates via the hydrothermal method. ZnO nanorods/nanowires are the most attractive nanostructures for the nanotechnology. Moreover, by doping TM into the ZnO cause change to its properties and enhanced the ferromagnetic properties at room temperature. In this work, we mainly investigated on controlled synthesis of ZnO nanorods and TM-doped ZnO nanorods. The ZnO nanorods have been chosen in this work due to its unique structural and physical properties along with their simple growth steps using the hydrothermal method. Then, this was followed by characterization techniques and finally device fabrications and measurements. The details of the synthesis methods are provided in the following sections.

4.1.1 Hydrothermal synthesis of ZnO nanorods

4.1.1.1 Synthesis of ZnO nanorods mediated by HMT

In solution growth procedures of nanocrystals, there are two processes: the nucleation and the growth of the nanocrystals. The growth processes of ZnO nanorods/nanowires consists of the following procedures: preparation of substrate, seeding, preparation of precursor solution and growth processes [1-6]. In this dissertation, the ZnO nanorods were grown on a number of thin films of metal coated glass, glass, semiconductor and polymer coated substrates.

Prior to the solution growth procedures, the substrates were sequentially and repeatedly immersed in isopropanol under sonication for 5 minutes to eliminate organic contaminant and unwanted particles. This cleaning step is followed each time by rinsing the substrates in de-ionized water (DI water) and finally the substrates were blown dried by nitrogen gun and dried in air at room temperature (RT).

In a typical process, the seed layer was spun coated three times with a seed solution (ZnO nanoparticles) at 3000 revolutions per minute (rpm) for 30s and then the samples were annealed in a preheated oven at 120^{o}C for 10 minutes. The main benefits for using ZnO nanoparticles as the seed layer in the hydrothermal growth method is to provide nucleation sites for ZnO nanorods. Also, the ZnO seed layer was found to be a critical factor for alignment and uniformity of the grown ZnO nanorods [7]. The seed solution was prepared by dissolving zinc acetate dehydrate ($C_4H_{10}O_6Zn$) in absolute methanol (99%) to obtain 0.01 M concentration

under stirring at 60ºC on a hotplate and then followed by adding dropwise a solution containing potassium hydroxide (KOH) in methanol under vigorous stirring for 2 hours [7].

In the precursor solution preparation process of ZnO nanocrystals, the most commonly used chemical agents to synthesize of ZnO nanorods/nanowires are zinc nitrate hexahydrate ($Zn(NO_3)_2 \cdot 6\,H_2O$) and hexamethylenetetramine (HMT) ($C_6H_{12}N_4$) [1-7]. In general, the precursor solution prepared by mixing equimolar of zinc nitrate hexahydrate and HMT under stirring for one hour [2].

The final process is the hydrothermal growth process. The ZnO seed-layers attached to the substrates were immersed horizontally in the growth solution and kept in a preheated oven at 90ºC. Then the samples were collected after different growth durations and cleaned with DI water and dried at RT for further characterizations and device fabrication processes. For most of the case in this work, 0.075M concentration of the solution has been selected. The reaction processes involved in this method are described as the following [1-7]:

$$C_6H_{12}N_4 + 6H_2O \leftrightarrow 6HCHO + 4NH_3 \quad (4.1)$$

$$NH_3 + H_2O \rightarrow NH_4^+ + OH^- \quad (4.2)$$

$$Zn(NO_3)_2 \rightarrow Zn^{2+} + 2NO_3^- \quad (4.3)$$

$$Zn^{2+} + 4NH_3 \rightarrow Zn(NH_3)_4^{2+} \quad (4.4)$$

$$Zn^{2+} + 4OH^- \rightarrow Zn(OH)_4^{2-} \quad (4.5)$$

$$Zn(NH_3)_4^{2+} + 2OH^- \rightarrow ZnO + 4NH_3 + H_2O \quad (4.6)$$

$$Zn(OH)_4^{2-} \rightarrow ZnO + H_2O + 2OH^- \quad (4.7)$$

In addition for well-aligned and uniform size distribution of ZnO nanorods, the rapid mixing is applied in order to get a homogenous solution or monodisperse nanoparticles. To obtain reasonable mono-dispersed nanoparticles for nucleation, the precursor solution should be designed in such a way that the nucleation occurs with the formation of huge amount of nuclei in a relatively short time [8]. Generally, the synthesis is carried out by injecting one chemical compound into the remaining ones within a very short time [8]. In this work, a solution of Zn ions and an equimolar concentration of HMT solution were separately prepared in DI water. Then both transparent solutions were rapidly mixed with a flow rate of 10 ml/s by injecting the HMT solution into the Zn ions solution under continuous stirring. The transparent Zn ions solution immediately changed to a translucent whitish color within 1 to 5 seconds due to the rapid hydrolysis of the zinc complexes in the growth solution. Then the mixed solution

was kept under continuous stirring at room temperature for 15 minutes. Then the final process followed by the hydrothermal growth process.

4.1.1.2 Synthesis of ZnO nanorods mediated by Ammonia

The developed solution growth method here represents a fast and simpler method for the growth of the ZnO nanorods. This is due to the fact that this method does not required seed layers coated on the substrates. So, the substrates can be used for the growth of ZnO on it directly after cleaning. In this experiment, ammonia rapidly reacts with water to produce ammonium hydroxide, which provides a continuous source of OH^- for hydrolysis and aids the precipitation of the final products. The rapidly mixed ammonia into the nutrient solution facilitates the homogeneous nucleation of ZnO on the substrate [9-10]. Therefore, when there is enough ammonia content in the nutrient solution, nuclei of ZnO crystals are formed on the substrates and dense ZnO nanorods would be produced over a large area.

The growth procedure is described as the following: substrates preparation, precursor solution preparation and growth process. The substrates preparation and growth processes are performed as mentioned in the growth procedure of ZnO nanorods mediated by HMT above. While the precursor solution preparation process is done by mixing 0.075 M concentration of zinc nitrate hexahydrate $[Zn((NO)_3)_2 \cdot 6H_2O]$ in DI water, using magnetic stirring of the mixture in a beaker. Then, ammonia solution was rapidly mixed into the zinc nitrate hexahydrate precursor solution until the solution pH reached 9 under stirring at room temperature for one hour. In addition, ammonia will lead to form zinc ionic complexes, which are absorbed on the side planes of the ZnO nanorods. This would lead to suppress the growth velocity of the side surfaces [10-12]. The expected chemical reactions and the generation of zinc ionic complexes are given as the following equations:

$$NH_3 \cdot H_2O \leftrightarrow NH_4^+ + OH^- \tag{4.8}$$

$$OH^- + Zn^{2+} \rightarrow Zn(OH)_2 \tag{4.9}$$

$$Zn(OH)_2 \xrightarrow{\Delta} ZnO(s) + H_2O \tag{4.10}$$

$$Zn^{2+} + nNH_3 \leftrightarrow Zn(NH_3)_n^{+2}, \text{n} = 1, 2, 3 \text{ or } 4 \tag{4.11}$$

The substrates used in this work were metals coated glass (gold and silver coated glass), semiconductor (p-type Si) and flexible PEDOT:PSS coated on plastic.

4.1.2 Synthesis of TM-doped ZnO nanorods

As mentioned in the previous chapters, the hydrothermal method is considered as a promising method due to low cost, environmental friendly, ease of fabrication, large scale production, and the properties of the materials can be controlled by the growth parameters and precursor preparation conditions. However, the synthesis of TM-doped ZnO with controlled shape, structure, and uniformity on any substrates remains a challenge. Therefore, the growth method developed here represents a new and simple method which maintains the nanorods structures with high incorporation of dopant concentration. We investigated TM-doped ZnO nanorods synthesized via both mediated by HMT and ammonia. The synthesis method for TM-doped ZnO nanorods are almost the same as ZnO nanorods, including substrates preparation, seeding process, precursor solution preparation and growth process. The only different is the precursor solution preparation process. Therefore, the next section describes the solution preparation process for synthesis of the TM-doped ZnO nanorods.

4.1.2.1 TM-doped ZnO nanorods mediated by HMT

In the HMT mediated method, the preparation of the precursor solution for growing Mn-doped ZnO nanorods is described as the following:

Firstly, an aqueous solution **A** is prepared by mixing of equimolar (0.075 M) of zinc nitrate hexahydrate and HMT in DI water. Secondly, a diluted solution **B** is a solution of Mn ions prepared by dissolving a specific percentage of $[MnCl_2 \cdot 6H_2O]$ in DI water contained of 20 percent ethanol. Thirdly, the solutions **A** and **B** were mixed then homogenized by ultra-sonication bath for 1 hour and continuously stirred for another 1 hour at RT. Finally, the ZnO seed-layers coated substrates were placed horizontally in the growth aqueous solution and kept in a preheated oven for 5 hours at 80^{o}C. When the growth was completed, the samples were washed with DI water and dried at RT.

4.1.2.2 TM-doped ZnO nanorods mediated by Ammonia

In the ammonia mediated method, the preparation of the precursor solution for growing Mn-doped ZnO nanorods and Fe-doped ZnO nanorods are described as follow:

- **For Mn-doped ZnO nanorods**

Firstly, 0.075 M precursor solution was prepared by mixing $[Zn((NO)_3)_2 \cdot 6H_2O]$ and a specific atomic concentration of $[Mn((NO)_3)_2 \cdot 6H_2O]$ in DI water under stirring for 2 hours. Secondly, the ammonia solution is rapidly added into the above mixed solution which reached a pH = 10 and this growth solution was kept under magnetic stirring for 30 minutes at RT.

Finally, the prepared ZnO seed-layers substrates were placed horizontally in the growth solution and kept in a preheated oven at 90^{o} C for 6 hours.

- **For Fe-doped ZnO nanorods**

Zinc nitrate hexahydrate, iron (II) chloride tetrahydrate and iron (III) chloride hexahydrate were used as precursors. The growth solution was prepared by mixing of 0.075 M of zinc nitrate hexahydrate and a specific concentration of the iron source prepared by iron ions $[Fe^{+2}]$:$[Fe^{+3}]$=1:2 in DI water. Then the growth solution was subsequently stirred for 1 hour at RT and ammonia solution is added drop-wise to the growth solution, resulting in an orange solution with a pH = 9.3. This solution was kept under magnetic stirring for another 1 hour at RT. In this adopted approach, ammonia was used to tailor the pH value in the growth solution and used to facilitate the growth of ZnO nanocrystals. When there is enough of ammonia content in the growth solution, the nuclei of ZnO nanocrystals be formed rapidly on over the substrates and this provides dense and long ZnO NRs growth on over the large area of the substrate [10-11]. The high amount of ammonia contents used as additive to hydrolyze in the growth solution provide Fe ions doped in ZnO matrix without morphology deformation.

The schematic diagram of the hydrothermal synthesis of ZnO and TM-doped ZnO nanorods is simplified and shown as in Figure 4.1.

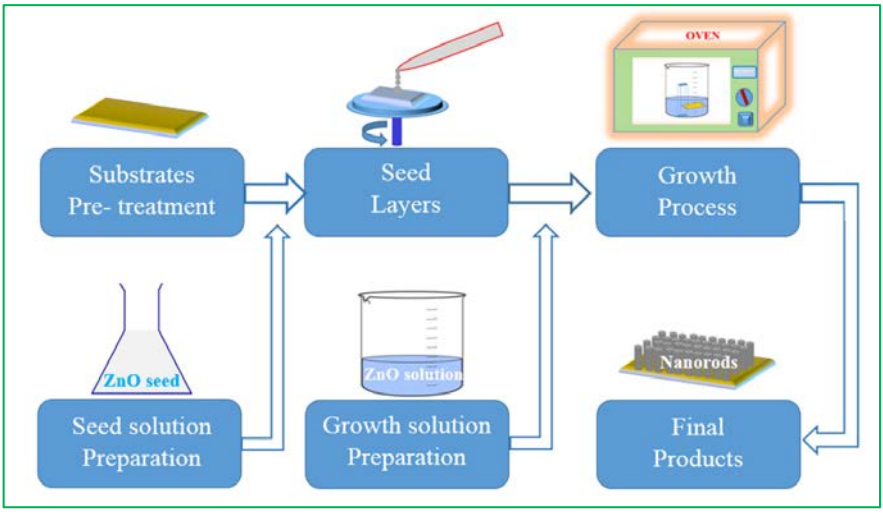

Figure 4. 1: *Schematic diagram of the hydrothermal growth of ZnO and TM-doped ZnO NRs.*

4.2 Characterization methods

After the growth process is completed, different characterization techniques were used to investigate the morphology, structure, electronic structure, optical properties and magnetic properties. Scanning electron microscope (SEM) was used to investigate the morphology of the samples. X-ray diffraction (XRD) is used to get the detailed information about the crystal structure of the samples. X-ray photoelectron spectroscopy (XPS) was used to investigate the electronic structure and the incorporation of the dopant in the samples. The optical properties were investigated by photoluminescence (PL), cathodoluminescence (CL) and UV-vis spectroscopies. Finally, the magnetic properties of the material was investigated by superconducting quantum interference device (SQUID) measurements. In this section, we will briefly introduce all these characterization techniques.

4.2.1 Morphological, structural and electronic structure characterizations

4.2.1.1 Scanning electron microscope

SEM is one of the most important instruments used for morphology analysis. The SEM generates images by scanning the samples using a focused electron beam. The electrons interact with atoms in the sample and produce various signals (surface information of the samples). The SEM utilizes a focused electron beam to scan across the surface of the samples then it systematically produces large numbers of signals and these electron signals are converted to a visual signal, which can be displayed on a screen [13]. The types of signals produced by a SEM include secondary electrons (SE), back-scattered electrons (BSE), characteristic X-rays, light (cathodoluminescence) (CL), specimen current and transmitted electrons. However, these types of signal are not usually present on a single machine and depend on the type of detector and its own specification. However, in all SEMs, secondary electron detectors are the most common mode of detection. When the primary beam strikes the surface of the sample, it causes ionization of specimen (atoms), loosely bound electrons may be emitted (secondary electrons). These electrons possess low energy (3-5eV), therefore, they possibly can move from a surface region within a few nanometers. So, secondary electrons accurately mark the position of the beam and give topographic information with good resolution [13]. The image of the surface is generated on the screen by scanning the sample and detecting the secondary electrons signals. In the present work, the SEM images were collected by secondary electron detector.

4.2.1.2 X-ray diffraction

X-rays diffraction (XRD) is a rapid and a powerful technique used to study the phase of a crystalline material, information on unit cell lattice parameters, crystal structure, crystal orientation and crystallite size [14]. XRD is widely used to characterize unknown crystalline materials. The working principle of the XRD technique is relied on constructive interference of X-rays and a crystalline sample [14]. In a crystal, the atoms distribute regular in space, which comes into being crystal lattices. These lattices form a series of parallel planes with spacing distance *d*. The x-rays are generated by a cathode ray tube (X-ray produced by the impact of accelerated electrons with heavy metal such as Cu), filtered (filtered and collimated by nickel filters) to produce monochromatic X-ray radiation which directed toward the sample. When X-rays light with wavelength λ is projected onto a crystal lattice at an angle θ, the interaction of the incident X-rays with the sample provides constructive interference if the conditions satisfy Bragg's law [15]:

$$n\lambda = 2d_{hkl}\sin(\theta) \tag{4.12}$$

where *n* is an integer 1, 2, 3….. (usually n =1), λ is wavelength in angstroms (1.5418 Å for CuK_{α}), d_{hkl} is spacing between the planes, the θ is the angle between the incident light and the lattice planes, the 2θ is angle between the incident and scattered beams, the angle 2θ of maximum intensity is called the Bragg angle. All diffraction directions of the lattice will be generate by scanning through a range of 2θ angles on the sample. Figure 4.2 illustrates the reflection of X-rays from two planes of atoms in a crystal solid. From these XRD pattern, the lattice parameter of the samples can be estimated by equations 4.13-4.15.

The direction of plane normal [*hkl*] is perpendicular to a plane of atoms and the diffraction vector **S** is the vector bisects the angle between the incident and diffracted beam [17]. The lattice constants '*a*' and '*c*' and the spacing d_{hkl} for the wurtzite structure of ZnO can be calculated using the relations [15-18]:

$$a = \sqrt{\frac{1}{3}}\frac{\lambda}{sin\theta} \tag{4.13}$$

$$c = \frac{\lambda}{sin\theta} \tag{4.14}$$

$$\frac{1}{d_{hkl}^2} = \frac{4}{3}\frac{h^2+hk+k^2}{a^2} + \frac{l^2}{c^2} \tag{4.15}$$

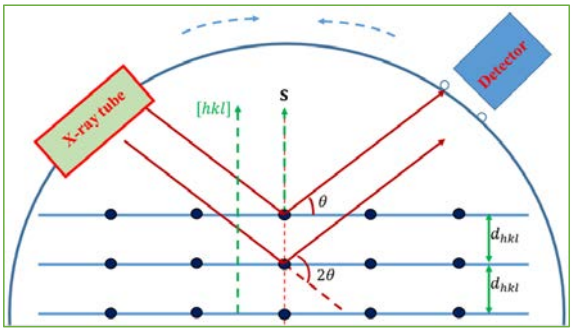

Figure 4. 2: *Typically Bragg Brentano geometry [15-18].*

4.2.1.3 X-ray photoelectron spectroscopy

X-ray Photoelectron Spectroscopy (XPS) is widely used to investigate the chemical composition of surfaces based on photo-ionization effect [19-20]. XPS uses to measure chemical composition at the surface (0 - 10 nm) of the sample, chemical or electronic state of each chemical element and uses to study the energy distribution from the emitted electrons at the surface [19-20]. In principle, the XPS spectra generated by radiated an X-rays beam on the samples. When the X-ray photon energy is higher enough, the core electron will escape from the atom at the surface of the sample and emit from the surface of the sample with certain kinetic energy, which is also called photoelectron. Then simultaneously the kinetic energy and amount of electrons that releases from the top of the material (0 - 10 nm) are measured [19]. In general, the energy of an X-ray with particular wavelength is known, and the kinetic energies of the emitted electrons are measured. The working principle of the XPS spectroscopy and binding energy diagram are illustrated in Figure 4.3.

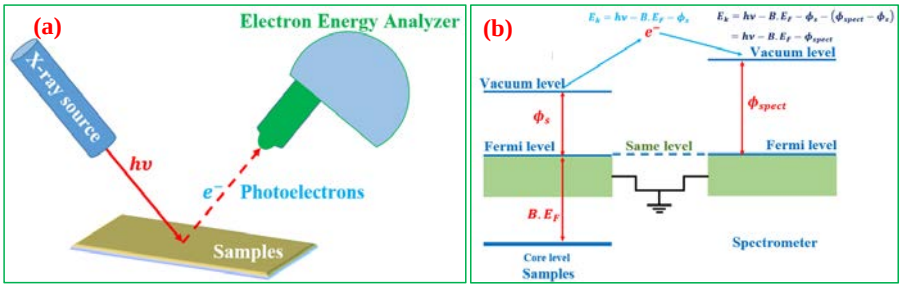

Figure 4. 3: *(a) The working principle of the XPS spectroscopy and (b) binding energy diagram [19].*

Therefore, the binding energy of each emitted electrons can be estimated by the following equations 4.16 and 4.17 [19-20]:

$$E_b = E_{phot} - \left(E_k + \phi_{spect}\right) \quad (4.16)$$

$$E_k = h\nu - E_b - \phi_{spect} \quad (4.17)$$

Where $E_b$is the binding energy (B.E) of the atomic orbital from which the electron originates, E_{phot} is the energy of the X-ray photons being used, E_k is the measured kinetic energy of the electron and ϕ_{spect} is the work function of spectrometer. The XPS spectrum describes about the amount of detected electrons as a function of binding energy of the detected electrons. Due to each element produces a set of XPS peaks at a specific characteristic binding energy values therefore the XPS normally used to analyze the concentration of the chemical elements on the surface of the sample. A change in the elemental binding energies (the chemical shifts) can be used to identify the chemical state of the materials [19-20].

4.2.2 Optical properties characterization

4.2.2.1 Photoluminescence spectroscopy

The photoluminescence (PL) spectroscopy is also an important technique for the investigation and characterization of the optical properties, electronic structure of semiconductors and defects occurring in materials [21]. The main principle of the PL measurements is that, the semiconductor is excited by light photons which has higher energy than the band gap of the semiconductor such as a laser. Then the incident photons are absorbed and create electron-hole pairs in the semiconductor. Within a short period of time the electron-hole pairs are recombined and emit photons from the semiconductor, the energy of the emitted photons reflects the carrier energy in the semiconductor. Finally, the emitted luminescence (light) and intensity are collected and recorded to generate a PL spectrum. These emitted photoluminescence and intensity are the direct measurement of the semiconductor properties such as bandgap, impurity levels and defect detection and recombination mechanisms [21].

4.2.2.2 Cathodoluminescence spectroscopy

The cathodoluminescence (CL) technique is similar to other spectroscopic techniques such as PL spectroscopy technique. Comparing the CL spectrum with PL spectrum should yield similar results. In principle, the electron beam excites the sample, leading to the emission of light from the semiconductor sample, showing all mechanisms of radiative recombination which are present. CL spectroscopy is used to investigate the impurity induced defects, trace element analysis, and to map the spatial distribution of stress around defects. An advantage of using the CL is the ability to obtain more detailed depth-resolved information by varying the

electron-beam energy [22-23]. In this work, the CL spectra were characterized by using Mono CL 4 system integrated with LEO 1550 Gemini SEM equipped with a fast charge-coupled device (CCD) detection system and Peltier cooled photomultiplier tube for signal acquisition at an accelerating voltage of 10 kV.

4.2.2.3 UV-visible spectroscopy

Ultraviolet-visible spectroscopy (UV-vis) is a spectroscopy (absorption or reflectance) in the ultraviolet-visible region. The UV-vis absorption spectroscopy provides information of light absorption as a function of wavelength, which describes the electronic transitions occurring in the measured samples. The UV-vis spectrophotometer detects the light intensity passing through a sample and compares the detected intensity to incident light intensity (light before passes through the sample) [24]: The absorbance *A* is simple expressed as Beer's law:

$$A = -log\left(\frac{I}{I_0}\right) \tag{4.18}$$

Where the ratio I/I_0 is called *transmittance*, I is the intensity of light passing through the sample and I_0 is the intensity of light before passing through the sample. In this work, the optical band gap of the grown samples were estimated using the following equation [15]:

$$\alpha = \left(\frac{k}{h\upsilon}\right)\left(h\upsilon - E_g\right)^{\beta} \tag{4.19}$$

Where $\alpha = 2.303 \times (\frac{A}{d})$ is the absorption coefficient, d is thickness of the sample (length of nanorods), β=1/2 for direct band gap semiconductors and k=αλ/4π is the extinction coefficient, h is Planck's constant and $h\upsilon$ is the incident photon energy [25].

$$\alpha = \left(\frac{k}{h\upsilon}\right)\left(h\upsilon - E_g\right)^{1/2} \tag{4.20}$$

$$(\alpha h\upsilon)^2 = C(h\upsilon - Eg\,) \tag{4.21}$$

The optical energy gap of the samples were obtained from the intercept of the linear portion with the x-axis of $(\alpha h\upsilon)^2$ versus $h\upsilon$ curve.

4.2.3 Magnetic properties characterization

The physical quantity called magnetic susceptibility (χ_m) describes the properties of the material placed in external magnetic field. Magnetic susceptibility is defined as [26]:

$$M = \chi_m H \tag{4.22}$$

Where M is magnetization of the material in the magnetic field and H is the field intensity. While the $\chi_m \gg 1, -1 < \chi_m < 0,$ and $0 < \chi_m \ll 1$ the material is classified as ferromagnetic materials, diamagnetic materials and paramagnetic materials, respectively. Normally,

magnetization is measured by using superconducting quantum interferometer device (SQUID) magnetometer. This is due to the fact that the SQUID provides extremely high sensitivity to any magnetization such as magnetic impurities, precipitates, clusters, and mixed magnetic phases. In the case of TM-doped ZnO materials, SQUID measurement is performed to observe the ferromagnetism behavior at Curie temperatures near/above room temperature [27]. The combination of SQUID, XRD and XPS measurements can provide information about the origin of ferromagnetism of the TM-doped ZnO nanostructures. In this work, the origin of the RT ferromagnetism of Fe-doped ZnO are performed by the combination of SQUID, XRD and XPS measurements.

4.3 Device fabrications and measurements

After synthesis and characterization processes, the synthesized samples have been used to fabricate biosensors to detect the creatinine concentration and indirectly determine the mercury chemical compound, piezoresistive sensors, and UV photodetectors.

4.3.1 Potentiometric biosensors

As mention in the previous chapter, there are different types of the biosensors. In this work, potentiometric biosensor have been selected. This is due to the fact that the potentiometric technique is friendly for living biological samples, only the accumulation of charge is measured and minimum hardware is required. The fabrication processes of the potentiometric biosensor are divided into three steps: the electrodes preparation, enzyme immobilization and electrochemical measurement.

- **Electrode preparation process**

The ZnO-NRs arrays electrode, called working electrode was prepared by growing the ZnO nanorods on gold coated glass substrates by using the low temperature hydrothermal approach which HMT is used as the mediator during the growth. It should be noted that at the top of the gold coated glass substrates were partially covered which preserved to use as contact area.

- **Enzyme immobilization process**

The recognition element (enzyme) was immobilized on the ZnO nanorods arrays by using the electrostatic physical adsorption technique. The enzyme was electrostatically immobilized on the electrodes by dipping the ZnO nanorods grown on Au coated glass electrodes into the enzyme solution for 5 minutes then dried in air for 1 hour at RT. The immobilized electrodes were stored at 4°C in dry condition. This method was applied for the immobilization of enzyme on the ZnO-NRs electrode due to the chemical structure. Enzyme such as glucose oxidase

(GOD) and ZnO both possess polar atoms which can attracted each other through the electrostatic binding.

- **Electrochemical measurements**

All the potentiometric biosensor measurements were performed at RT by using a *pH* meter (Model 744, purchase from Metrohm). The Ag/AgCl electrode is used as the reference electrode and the response time of the biosensor was measured by a Keithly model 2400 series. The electrochemical reaction could produce charges near the surface of the working electrode which produces potential difference between biosensor working electrode and the reference electrode inside the electrolyte solution. The electrochemical response (electromotive force (EMF)) changed according to the change in concentration of ions in the target electrolyte solution. The EMF response of ion selective electrodes (biosensor) can be explained according to the Nernst's expression [28]:

$$E = E_0 + \frac{RT}{ne}\ln\left(\frac{[\mathrm{Ox}]}{[\mathrm{Red}]}\right) \tag{4.23}$$

Where E_o is the cell potential at standard-state conditions, E is the cell potential, T is the temperature (K), R is the ideal gas constant, e is the fundamental charge of electrons and n is the number of electrons transferred during the reaction. [Ox] is the concentrations of oxidized and [Red] is the concentration of the reduced species, respectively. The commonly log form of Nernst equation at 25^{o}C can be express [29]:

$$E = E_0 - \frac{0.059}{n}\log\left(\frac{[\mathrm{Red}]}{[\mathrm{Ox}]}\right) \tag{4.24}$$

Biosensors also can be used to detect some toxic chemical compounds by inhibition process of the enzyme activities. The inhibition between the enzyme and the heavy metal compound are either irreversible or reversible inhibition [30- 31]. In this work, the inhibition mechanism of glucose oxidase by mercury is reversible. The inhibitor binds to the enzyme is at a site other than the active site of the enzyme which makes a change to the shape of the enzyme. The phenomena leads to change the enzyme activity. The inhibition degree to the glucose oxidase is given by the following equation [30- 31]:

$$I\% = \left(\frac{I_0 - I}{I_0}\right) \times 100 \tag{4.25}$$

Where I % is the degree of inhibition, I_0 is the response to glucose during the absence of inhibitor and I is the response to glucose during the presence of inhibitor [30- 31]. Figure 4.4 illustrates the configuration of potentiometric biosensor and its measurements.

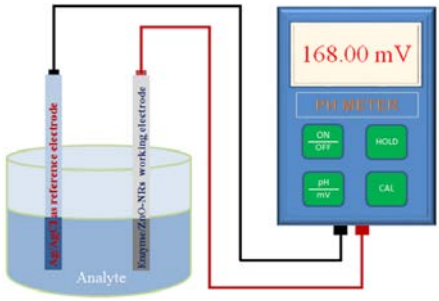

Figure 4. 4: *The configuration of potentiometric biosensor and its measurements.*

4.3.2 Schottky diode based piezoresistive sensor and UV photodetector

As mentioned in chapter 3, due to the fact that p-type ZnO is difficult to achieve which limits homojunction p-n junction based on ZnO. Therefore, metal-ZnO Schottky diodes based sensors are more attractive. Generally, Schottky contact or Ohmic contact with ZnO is solely determined by their work functions. Ideally, the formation of Ohmic contact between a metal and a semiconductor junction if the barrier formed by the contact is zero. For n-type semiconductor and in order to form an Ohmic contact, the work function of the metal must be close to or smaller than the electron affinity of the semiconductor, this is in contrast to the Schottky contact [32]. Schottky–Mott model, barrier height of metal-semiconductor junction is defined by the difference between metal work function and electron affinity of the semiconductor [33-34]. The schematic of a Schottky barrier junctions with energy level in the metal and n-type semiconductor are shown in Figure 4.5.

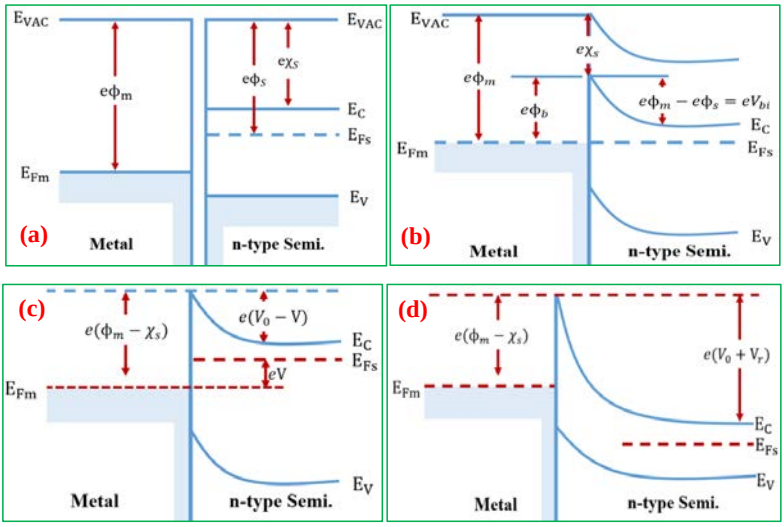

Figure 4. 5: *(a) The energy level in metal and semiconductor (b) the metal-semiconductor junction at equilibrium (c) band diagram of metal-n-type semiconductor under forward bias and (d) band diagram of metal-n-type semiconductor under reverse bias [34].*

The *I-V* characteristics of a Schottky diode can be written as [35-41]:

$$I = I_0 \exp\left(\frac{qV}{nkT}\right)\left[1 - \exp\left(\frac{-qV}{kT}\right)\right] \tag{4.26}$$

where q is the elementary charge, k is Boltzmann's constant, T is the absolute temperature, V is the applied voltage, n is ideality factor and I_0 is the reverse saturation current given by:

$$I_0 = AA^*T^2 \exp\left(\frac{-q\phi_B}{kT}\right) \tag{4.27}$$

where A^* is the effective Richardson constant (theoretically 32 A/cm^2 K^2), A is the Schottky contact area and ϕ_B is the barrier height. Under forward bias, the ϕ_B and n can be estimated with a least-squares fit to equation (4.27) and to the slope of the ln(I/[1-exp(-qV/kT)]) versus V plot [35, 37].

In this work, materials such as Au, poly(2,3-dihydrothieno-1,4-dioxin)-poly(styrenesulfonate) (PEDOT:PSS) were used as the materials to form the Schottky contact with ZnO and alloy Ti/Au, fluorine doped tin oxide (FTO) and Ag materials are used to form the Ohmic contact with ZnO. Then the fabricated sensors based Schottky diodes are used for piezoresistive sensors and UV photodetectors. Figure 4.6 shows a schematic diagram of the ZnO nanorods and the TM-doped ZnO nanorods Schottky diode based devices for piezoresistive sensor and UV photodetector. The performance of the piezoresistive sensor was studied by the *I-V* characteristics of the fabricated Schottky diode under the application of different external forces. Also, the performance of the UV photodetector was investigated by its *I-V* curve under dark and under UV light at a wavelength of 365 nm with power density of 2 mW/cm^2.

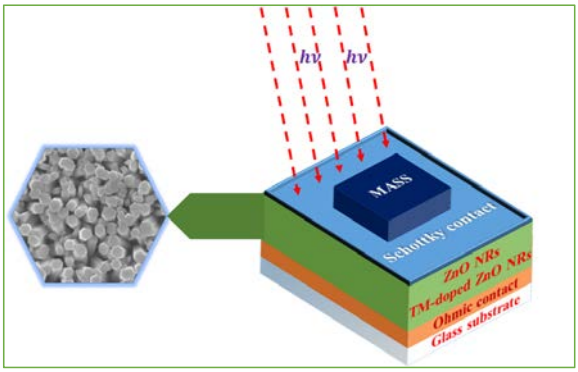

Figure 4. 6: *Schematic diagram of Schottky diode based on ZnO/TM-doped ZnO NRs.*

References

[1] M. Willander, L. L. Yang, A. Wadeasa, S. U. Ali, M. H. Asif, Q. X. Zhao and O. Nur, Zinc oxide nanowires: controlled low temperature growth and some electrochemical and optical nano-devices, *J. Mater. Chem.***19**, 1006-1018 (2009).

[2] M. Willander et al, Zinc oxide nanorod based photonic devices: recent progress in growth, light emitting diodes and lasers, *Nanotechnology* **20**, 332001(40 pages) (2009).

[3] G. Amin, M. H. Asif, A. Zainelabdin, S. Zaman, O. Nur, and M. Willander, Influence of pH, precursor concentration, growth time, and temperature on the morphology of ZnO nanostructures grown by the hydrothermal method, *Journal of Nanomaterials* **Volume 2011**, Article ID 269692 (9 pages) (2011).

[4] Z. L. Wang, ZnO nanowire and nanobelt platform for nanotechnology, *Materials Science and Engineering* **R 64**, 33-71 (2009).

[5] I. Udoma, M. K. Rama, E. K. Stefanakos, A. F. Hepp, D. Y. Goswami, One dimensional-ZnO nanostructures: Synthesis, properties and environmental applications, *MaterialsScienceinSemiconductorProcessing***16**, 2070-2083 (2013).

[6] S. Xu and Z. L. Wang, One-dimensional ZnO nanostructures: Solution growth and functional properties, *Nano Res.* **4(11)**, 1013-1098 (2011).

[7] A. Zainelabdin, S. Zaman, G. Amin, O. Nur, and M. Willander, Deposition of well-aligned ZnO nanorods at 50 C on metal, semiconducting polymer, and copper oxides substrates and their structural and optical properties, *Crystal Growth & Design*, **10**, 3250-3256 (2010).

[8] C. N. R. Rao, A. Muller, and A. K. Cheetham, Nanomaterials chemistry: Recent developments and new directions, *Wiley-VCH*, Weinheim (2007) p. 140.

[9] A. Ali Umar, M. Y. A. Rahman, R. Taslim, M. M. Salleh, and M. Oyama, A simple route to vertical array of quasi-1D ZnO nanofilms on FTO surfaces: 1D-crystal growth of nanoseeds under ammonia-assisted hydrolysis process, *Nanoscale Research Letters*, **2011**, **6:564** (12 pages) (2011).

[10] J. H. Tian, J. Hu, S. S. Li, F. Zhang, J. Liu, J. Shi, X. Li, Z. Q. Tian, and Y. Chen, Improved seedless hydrothermal synthesis of dense and ultralong ZnO nanowires, *Nanotechnology* **22**, 245601 (9 pages) (2011).

[11] X. L. Zhang, H. T. Dai, J. L. Zhao, S. G. Wang, and X. W. Sun, Surface-morphology evolution of ZnO nanostructures grown by hydrothermal method, *Cryst. Res. Technol.* **49**, 220-226 (2014).

[12] C. Xu, P. Shin, L. Cao, and D. Gao, Preferential growth of long ZnO nanowire array and its application in dye-sensitized solar cells, *J. Phys. Chem. C* **114**, 125-129 (2010).

[13] W. Zhou, R. Apkarian, Z. L. Wang, D. Joy, Fundamentals of scanning electron microscopy (SEM), Scanning microscopy for nanotechnology: Techniques and applications, *Springer*, New York (2007) pp. 1-40.

[14] http://serc.carleton.edu/research_education/geochemsheets/techniques/XRD.html, 10 October 2014.

[15] N. Shakti, P. S. Gupta, Structural and optical properties of sol-gel prepared ZnO thin film, *Applied Physics Research,* **Vol. 2, No. 1**, 19-28 (2010).

[16] http://www.absoluteastronomy.com/topics/X-ray_crystallography, 10 October 2014.

[17] http://prism.mit.edu/xray/oldsite/training.htm#chronological, 10 October 2014.

[18] M. Birkholz, Principles of X-ray Diffraction, Thin film analysis by X-ray scattering, *WILEY-VCH Verlag GmbH & Co. KGaA*, Weinheim, (2006) pp.10-11.

[19] http://mmrc.caltech.edu/SS_XPS/XPS_PPT/XPS_Slides.pdf, 7 October 2014.

[20] J. Chastain, and Roger C. King Jr., Introduction, Handbook of X-ray photoelectron spectroscopy, *Physical Electronics USA, Inc.*, (1995) pp.9-10.

[21] G. D. Gilliland, Photoluminescence spectroscopy of crystalline semiconductors, *Materials Science and Engineering* **R18**, 99-400 (1997).

[22] V. I. Petrov, Cathodoluminescence microscopy, *Physics-Uspekhi* **39 (8)**, 807-818 (1996).

[23] B. G. Yacobi, and D. B. Holt, Cathodoluminescence scanning electron microscopy of semiconductors, *J. Appl. Phys.* **59 (4)** (1986).

[24] Z. Chen et al, UV-vis spectroscopy, photoelectrochemical water splitting, *Springer Briefs in Energy* (2013) pp.49.

[25] P. Sharma, K. Sreenivas, and K. V. Rao, Analysis of ultraviolet photoconductivity in ZnO films prepared by unbalanced magnetron sputtering, *J. Appl. Phys.* **93**, 3963-3970 (2003).

[26] P. Marcon and K. Ostanina, Overview of methods for magnetic susceptibility measurement, *PIERS Proceedings*, Kuala Lumpur, MALAYSIA, March 27-30, (2012).

[27] H. Morkoc, and Ü. Özgür, ZnO-based dilute magnetic semiconductors, Zinc oxide fundamentals, materials and device technology, *WILEY-VCH Verlag GmbH & Co. KGaA*, Weinheim (2009) pp.278-339.

[28] D. A. Bernards, D. J. Macaya, M. Nikolou, J. A. De Franco, S. Takamatsu and G. G. Malliaras, Enzymatic sensing with organic electrochemical transistors, *J. Mater. Chem.***18**, 116-120 **(**2008).

[29] K. Khun, Z.H. Ibupoto, J. Lu, M.S. AlSalhi, M. Atif, A. A. Ansari, M. Willander, Potentiometric glucose sensor based on the glucose oxidase immobilized iron ferrite magnetic particle/chitosan composite modified gold coated glass electrode, *Sensors and Actuators B* **173**, 698-703 (2012).

[30] A. Amine, H. Mohammadi, I. Bourais, G. Palleschi, Enzyme inhibition-based biosensors for food safety and environmental monitoring, *Biosensors and Bioelectronics* **21**, 1405-1423 (2006).

[31] G. L. Turdean, Design and development of biosensors for the detection of heavy metal toxicity, *International Journal of Electrochemistry* **2011**, ID 343125 (15 pages) (2011).

[32] L. J. Brillson, and Y. Lu, ZnO Schottky barriers and Ohmic contacts, *J. Appl. Phys.* **109**, 121301 (33pages) (2011).

[33] O. Nur, M. Karlsteen, M. Willander, R. Turan, B. Aslan, M. O. Tanner, and K. L. Wang, Correlation between barrier height and band offsets in metal/ $Si_{1-x}Ge_x$/Si heterostructures, *Appl. Phys. Lett.* **73**, 3920-3922 (1998).

[34] E. V. Monakhov, A. Yu. Kuznetsov and B. G. Svensson, Zinc oxide: bulk growth, role of hydrogen and Schottky diodes, *J. Phys. D: Appl. Phys.* **42**, 153001 (17 pages) (2009).

[35] P. Klason1, O. Nur and M. Willander, Electrical characteristics and stability of gold and palladium Schottky contacts on ZnO nanorods, *Nanotechnology* **19**, 475202 (5 pages) (2008).

[36] U. Grossner, S. Gabrielsen, T. M. Børseth, J. Grillenberger, A. Yu. Kuznetsov, and B. G. Svensson, Palladium Schottky barrier contacts to hydrothermally grown n-ZnO and shallow electron states, *Applied Physics Letters* **85**, No. 12, 2259-2261 (2004).

[37] H. Noor, P. Klason, S. M. Faraz, O. Nur, Q. Wahab, M. Willander, and M. Asghar, Influence of background concentration induced field on the emission rate signatures of an electron trap in zinc oxide Schottky devices, *J. Appl. Phys.* **107**, 103717 (5p) (2010).

[38] G. Amin, I. Hussain, S. Zaman, N. Bano, O. Nur, and M. Willander, Current-transport studies and trap extraction of hydrothermally grown ZnO nanotubes using gold Schottky diode, *Phys. Status Solidi A* **207**, 748-752 (2010).

[39] R. Schifano, E. V. Monakhov, J. S. Christensen, A. Yu. Kuznetsov, and B. G. Svensson, Schottky contacts to hydrogen doped ZnO, *Phys. Status Solidi (a)* **205**, No. 8, 1998–2001 (2008).

[40] S. N. Das, J. H. Choi, J. P. Kar, K. J. Moon, T. I. Lee, and J. M. Myoung, Junction properties of Au/ZnO single nanowire Schottky diode, *Appl. Phys. Lett.* **96**, 092111 (3pages) (2010).

[41] M. Nakano, A. Tsukazaki, R. Y. Gunji, K. Ueno, A. Ohtomo, T. Fukumura, and M. Kawasaki, Schottky contact on a ZnO (0001) single crystal with conducting polymer, *Appl. Phys. Lett.* **91**, 142113 (3pages) (2007).

Chapter 5: Results and discussions

In this dissertation, we divided our results into two main parts. The first part (paper I-IV) is the synthesis of ZnO nanorods, their characterizations and the application of ZnO nanorods for detection of creatinine and mercury concentrations and piezoresistive sensor. The second part (paper V-VII) presents the growth, characterization of Mn-doped ZnO nanorods and Fe-doped ZnO nanorods and their applications as piezoresistive sensor and UV photodetectors.

5.1 Synthesis, characterization of ZnO NRs and their sensing applications

5.1.1 Seed-free hydrothermal synthesis of ZnO NRs (Paper I)

There are two processes for synthesis nanocrystals via the solution growth method, which are nucleation process and diffusion process of the growth of the nanocrystals [1]. The seedless hydrothermal synthesis of ZnO nanorods has been improved by introducing an ammonia or organic compound into the nutrient solution prepared by mixing zinc nitrate hexahydrate and HMT. The ammonia used here to facilitate the high density nucleation of ZnO on the substrate instead of using the seed layer [2]. We have developed and adopted a method for fast and low cost synthesis method for growing ZnO nanorods, which facilitates the homogeneous nucleation of ZnO on the substrate [2-3]. The ammonia content was added until the final nutrient solution has reached a pH of 9.3, which results in forming the nuclei of ZnO crystals on the substrates. Then the growth process was followed by placing different types of substrates (metals, semiconductor and polymer) in any direction in the final nutrient solution in a preheated oven at 90^{o}C. Finally, the morphology transformation, structural and optical properties of the grown samples were investigated. In Figure 5.1 (a-c), the SEM surface morphology images of ZnO samples grown at 1 hour, 4 hours and 6 hours have a morphology of pencil-like, truncated pencil-like, and rod-like morphologies, respectively. While Figure 5.1 (d-f) show ZnO nanorods that can be grown on Au coated glass, Ag coated glass and PEDOT:PSS, respectively [4]. The XRD measurement was performed for structure characterization and the optical band gap was obtained by UV-vis spectroscopy. Figure 5.2 shows the XRD patterns of the ZnO nanostructures grown on p-type Si wafer for 2, 4 and 6 hours and Figure 5.3 presents the UV-vis spectra of the ZnO nanostructures obtained for different growth durations. The XRD spectra show that the diffraction peak corresponding to the (002) planes is increasing as the growth duration has increased, which indicates that the ZnO nanorods are growing with an orientation along the *c-axis*. The optical energy band gap

of the ZnO nanorods grown at 2, 4, and 6 hours are estimated to be 2.8, 3.1 and 3.24 eV, respectively.

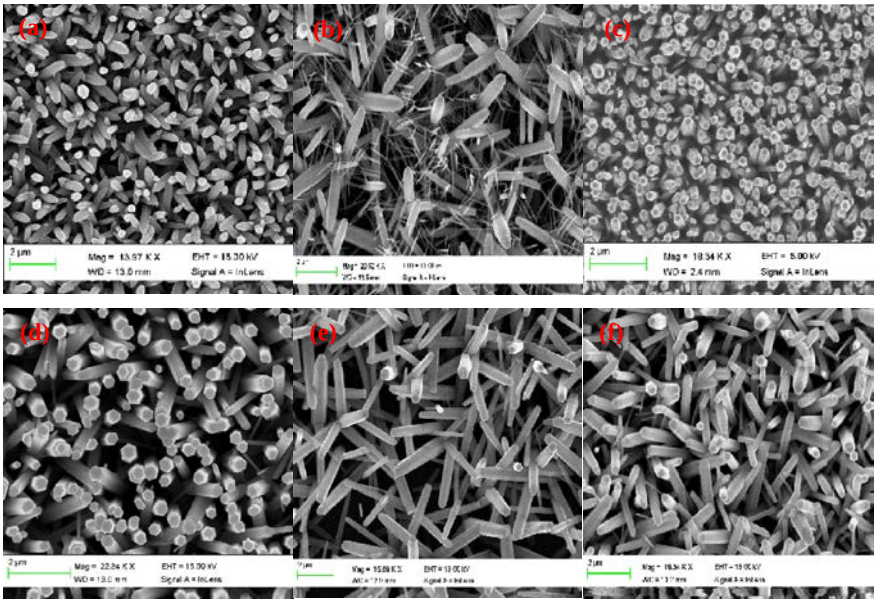

Figure 5. 1: *SEM images of ZnO growth (a) at 1 hour (b) at 4 hours (c) at 6 hours (d) on Au coated glass (e) Ag coated glass and (f) PEDOT:PSS coated plastic [4].*

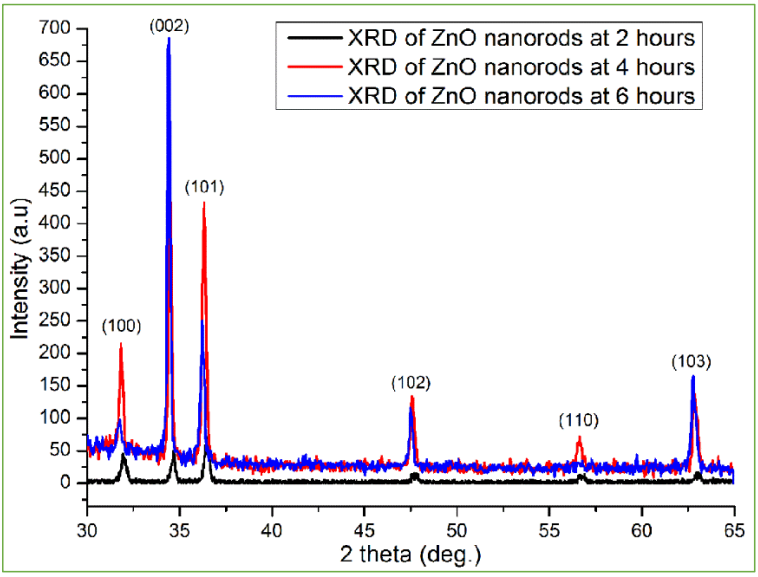

Figure 5. 2: *XRD pattern of ZnO nanocrystals grown at 2, 4 and 6 hours [4].*

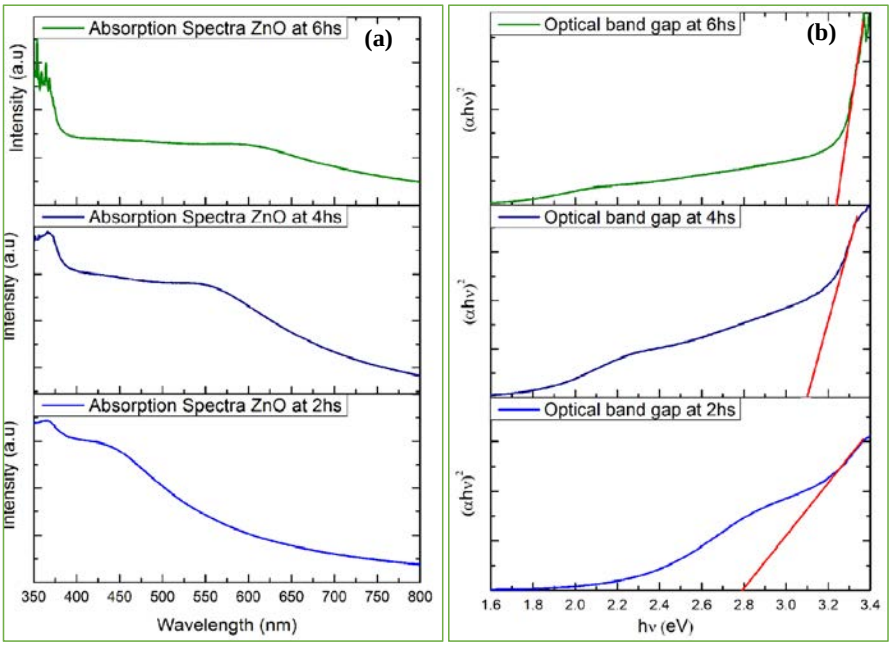

Figure 5. 3: *(a) UV-vis spectra of ZnO nanostructures grown at 2, 4 and 6 hours and (b) their optical band gaps [4].*

Therefore, this method demonstrated a fast and low cost synthesis procedure for synthesizing ZnO nanorods with controllable morphology, size and structure on any types of large area substrate.

5.1.2 ZnO NRs based piezoresistive sensor synthesized by rapid mixing hydrothermal method (Paper II)

ZnO nanorods on large area samples with uniform size distribution and high degree of alignment were synthesized for piezoresistive sensor application. The well-aligned and uniform size distribution of ZnO nanorods play an important role in achieving an improved performance of different devices [5]. In this work, well-aligned ZnO nanorods can be synthesized by the rapid mixing hydrothermal method. The growth procedure can be described in three steps: seeding process, homogenous solution preparation process and the hydrothermal growth process. In a typical process, the seed layer was spun coated three times using a seed solution that has been prepared using zinc acetate ($C_4H_{10}O_6Zn$) solution in ethanol [6] at 3000 rpm for 30s and then the ZnO seed-layers coated substrates were annealed in a preheated oven

at 120ºC for 10 minutes. In nutrients solution preparation process of ZnO nanocrystals, the most commonly used chemical agents such as zinc nitrate hexahydrate and HMT and they were also used in the present study [7-8]. In order to prepare a homogenous solution, rapid mixing has been applied by rapidly injecting the HMT solution into the Zn ions solution with a flow rate 10 ml/s. The solution of Zn ions and an equimolar concentration of HMT solutions were separately prepared in DI water. Finally, the hydrothermal growth process was perform normally by horizontally immersed the ZnO seed-layers coated substrates in the growth solution and it was kept in a preheated oven at 90ºC. Figure 5.4 (a) and (b) show SEM images of well-aligned and uniform size distribution of ZnO nanorods grown at 3 and 5 hours, respectively. The diameter of the grown ZnO nanorods were approximately 300 nm over the entire samples. In this experiment, 0.075 M of the growth solution is used.

The structural characterization of the ZnO nanorods was shown in Figure 5.5. (a). The XRD spectra of the ZnO nanorods grown at 3 and 5 hours located at 2θ values between 30°-65° are well consistent with the hexagonal phase of pure ZnO diffraction peaks (JCPDS #800075). The peaks at (002) plane is increasing as the growth duration was increased, indicating that the ZnO nanorods grown with a dominant orientation along the *c-axis* as the growth duration is increased. The optical emission of the ZnO nanorods was performed by room temperature CL as shown in Figure 5.5 (b). It is noted that the optical emission intensities increased with increasing the growth duration. The increase of the growth duration can improve the crystal quality of the ZnO nanorods [9]. The result is in good agreement with our XRD results.

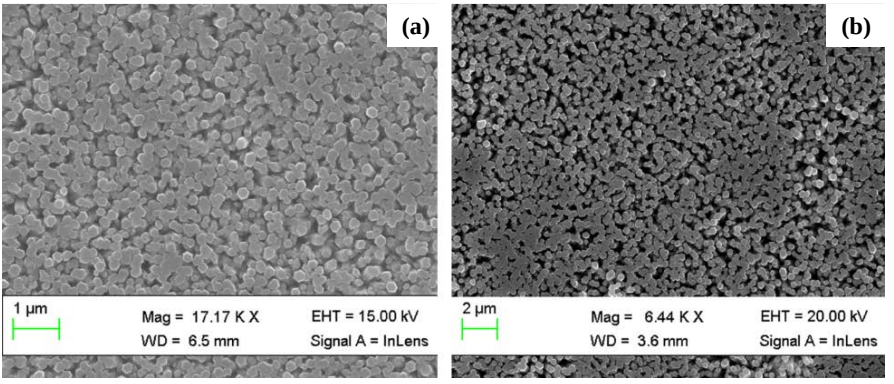

Figure 5. 4: *Typical SEM images of the ZnO NRs grown for (a) 3 hours and (b) 5 hours.*

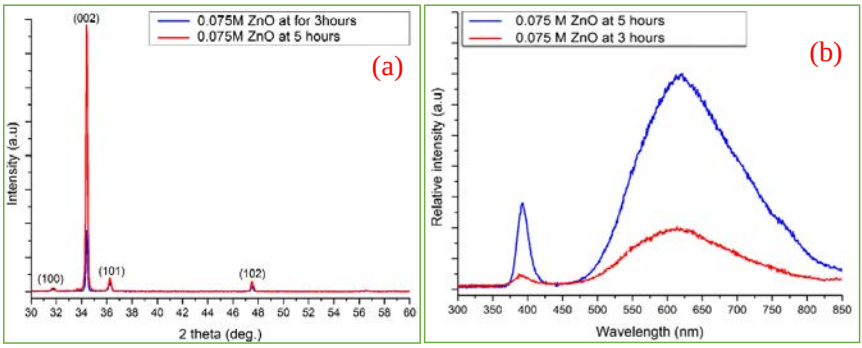

Figure 5. 5: *(a) The XRD pattern of ZnO nanorods grown for 3 and 5 hours and (b) Room-temperature CL spectra of the ZnO nanorods grown at 3 and 5 hours.*

The ZnO nanorods grown for 5 hours have been selected to fabricate a Schottky diode by gently pressed Au-coated plastic sheet onto the top of the ZnO nanorods grown on Ag-coated glass substrate. This fabricated Schottky diode was used as a sensitive piezoresistive sensor. The sensor provides high sensitivity and fast response time of S = 0.033 KPa^{-1} and 0.088 s, respectively. Figure 5.6 shows the schematic diagram of the fabricated piezoresistive sensor, *I-V* characteristics of the device under different loads, the electronic resistance variation ratios versus applied pressure, and the response and recovery times.

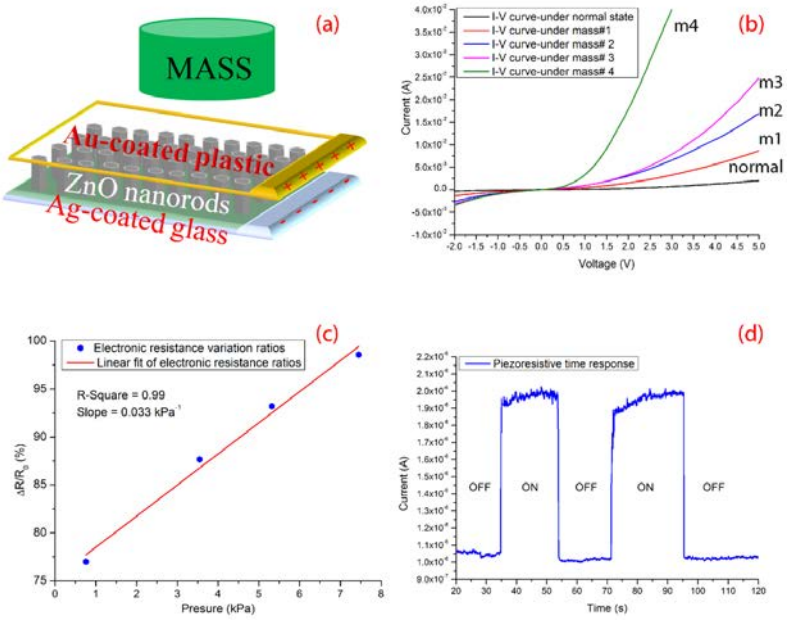

Figure 5. 6: *The schematic diagram and performance of the fabricated piezoresistive sensor.*

5.1.3 Potentiometric creatinine biosensor based on ZnO NWs (paper III)

1-D ZnO nanostructures possess wide band gap (3.37 eV at RT), high surface area to volume ratio, high catalytic efficiency, nontoxicity, biocompatibility, having high ionic bonding (60%), chemical stability and strong adsorption ability due to the high isoelectric point (IEP ~9.5) and insoluble at biological pH [10-12]. From these properties, 1-D ZnO nanostructures can be used for the direct adsorption and the interaction with desirable enzymes, providing a fast electron transfer directly between the enzyme's active sites and the electrode. In this work, potentiometric creatinine biosensor fabricated by immobilization of the creatinine deiminase (CD) enzyme and a chitosan membrane in conjunction with a glutaraldehyde on the surface of ZnO nanowires is demonstrated. SEM surface morphology images of the fabricated electrodes before enzyme immobilization, before use and after used are shown in Figure 5.7 (a-c).

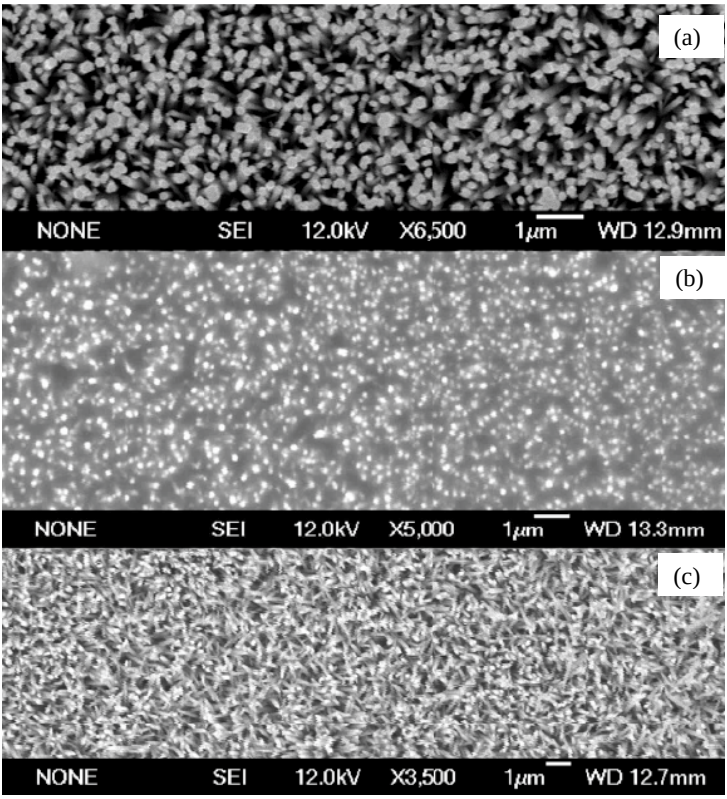

Figure 5. 7: *The SEM images of ZnO nanowires: (a) before immobilized CD enzyme, (b) after immobilized CD and (c) the sensor electrode after used [10].*

The electrochemical measurements of the creatinine biosensors based on an enzymatic reaction catalyzed by CD is given by [13]:

$$\text{Creatinine} + H_2O \xrightarrow{CD} N - Methylhydantoin + NH_4^+ \quad (5.1)$$

The electrochemical potential can be described by the equation:

$$ZnOs|Zn^{+2}\ \text{PBS sol}||Ag/AgCl\ \text{PBS sol}|Ag \quad (5.2)$$

The potentiometric response (EMF) of the biosensor changed according to the electrolyte's concentration following the Nernst's expression.

The potentiometric response shows a wide dynamic range of the output response (EMF) linear *vs.* the logarithmic concentrations of the creatinine with sensitivity of 33.9 mV/decade and 7 s response time. The calibration curve and reproducibility curves are shown in Figure 5.8. While the time response of the biosensor is shown in Figure 5.9. The developed biosensor is suitable for detection in small volumes with high sensitivity, good selectivity, fast response time, reproducibility, and wide dynamic range of operation.

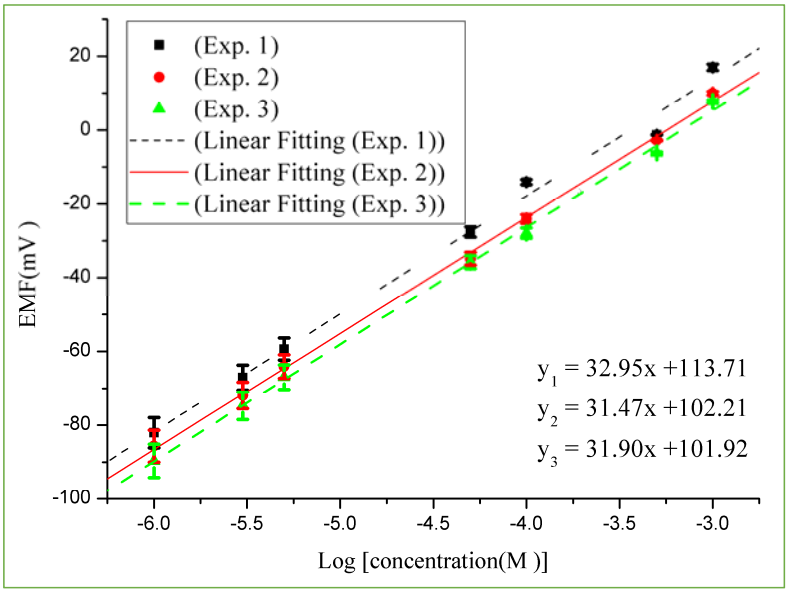

Figure 5. 8: *Calibration curves from three different experiments using the same sensor electrode versus Ag/AgCl reference electrode [10].*

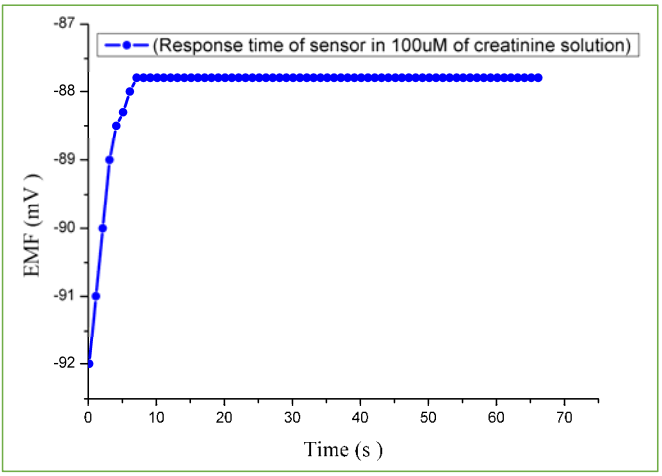

Figure 5. 9: *Time response of the creatinine sensor in 100 μ M creatinine solution [10].*

5.1.4 Indirect determination of mercury ion by inhibition of a glucose biosensor based on ZnO NRs (Paper IV)

Currently, a new and simple nanotechnology tool with high ability to monitor heavy metal with fast response time, inexpensive and on-site monitoring is needed. To fulfill these requirement, a biosensor is used as a useful analytical tools for indirect detection of chemical compound [14-16]. In this work, potentiometric glucose biosensor based on ZnO NRs used for indirect determination of mercury compound, resulting from the inhibition of mercury on an enzyme, called glucose oxidase (GOD). After growth of the ZnO NRs on Au coated glass substrate, GOD was immobilized on the surface of ZnO NRs by an enzyme solution containing of 1 mL of GOD solution (10 mg/ml of GOD in the PBS with a pH 7.4) and 1 mL of chitosan membrane. The chitosan was used as a matrix for the immobilization of GOD on ZnO NRs due to its excellent membrane forming ability, high permeability toward water, good adhesion, biocompatibility, non-toxicity and high mechanical strength [17]. The enzyme was electrostatically immobilized on the surface of ZnO NRs by dipping the ZnO NRs electrode into the enzyme solution above for 5 minutes and then the electrodes were dried in air at RT for 1 hour before use and stored in dry condition at 4°C when not in use. Figure 5.10 show the surface morphology images of the ZnO NRs electrodes before immobilization and after immobilization of GOD.

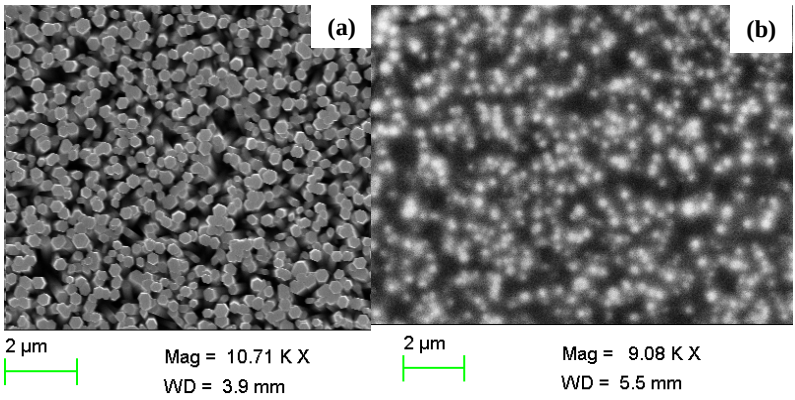

Figure 5. 10: *The SEM images of the ZnO NRs electrodes (a) before immobilization and (b) after immobilization GOD [18].*

Figure 5.11 (a) presents the glucose sensing mechanism, which shows the enzymatic reaction catalyzed by glucose oxidase (GOD) with *β-D-glucose* to produce the charged products of *gluconate*$^{-}$ and a proton (H^{+}). The EMF response to glucose concentration of this glucose biosensor can be explained by the Nernst's expression and the EMF response of the glucose biosensor was measured between the working electrode (GOD immobilized on ZnO NRs) and a reference electrode (Ag/AgCl) in glucose concentrations from 10^{-3} mM to 10 mM. Figure 5.11 (b) shows the output linear response versus the logarithmic glucose concentrations with a sensitivity of 41.9 mV/decade.

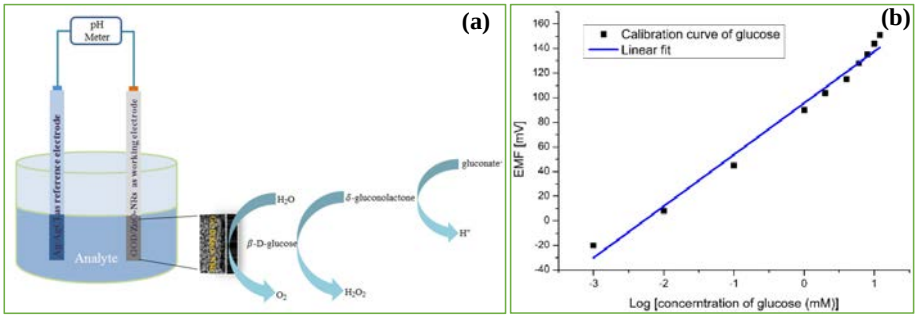

Figure 5. 11: *(a) The schematic diagram for the sensing mechanism and (b) the calibration curve for glucose concentrations [18].*

The enzyme–inhibitor (mercury ions) reaction have been investigated for the determination of Hg^{2+} ions by potentiometric glucose biosensor. Normally, the inhibition processes between the enzyme and the toxic compound can be reversible or irreversible inhibition. For GOD, the inhibition process with heavy metals is reversible, which makes the

inhibitor binds at a site other than the active site of the GOD, resulting in a changes in a shape of GOD that leads to a change in its activities. The inhibition degree to the GOD is given by $I\% = 100\left(\frac{I_0 - I}{I_0}\right)$, which I% is the degree of inhibition, $I_0$is the response to glucose in the absence of inhibitor, and *I* represents the response to glucose in the presence of inhibitor [18-19].

In this work, a low concentration of 1 mM of glucose in a standard phosphate buffer solution (PBS) is used and its stable EMF response was recorded (I_0) after that solutions of different concentrations of Hg^{2+} ions were added to inhibit the GOD activity and the change in the EMF response (*I*) was recorded. The results show that the biosensor has a linear range versus the logarithm of Hg^{2+} ion concentration of inhibition degree of the GOD. It can be divided into two linear parts as shown in Figure 5.12 (a-b). The first linear range is from 0.5×10^{-6}mM to 0.5×10^{-4}mM and the second linear range is from 0.5×10^{-4}mM to 20 mM. The biosensor response time is 8 s as presented in Figure 5.12 (c).

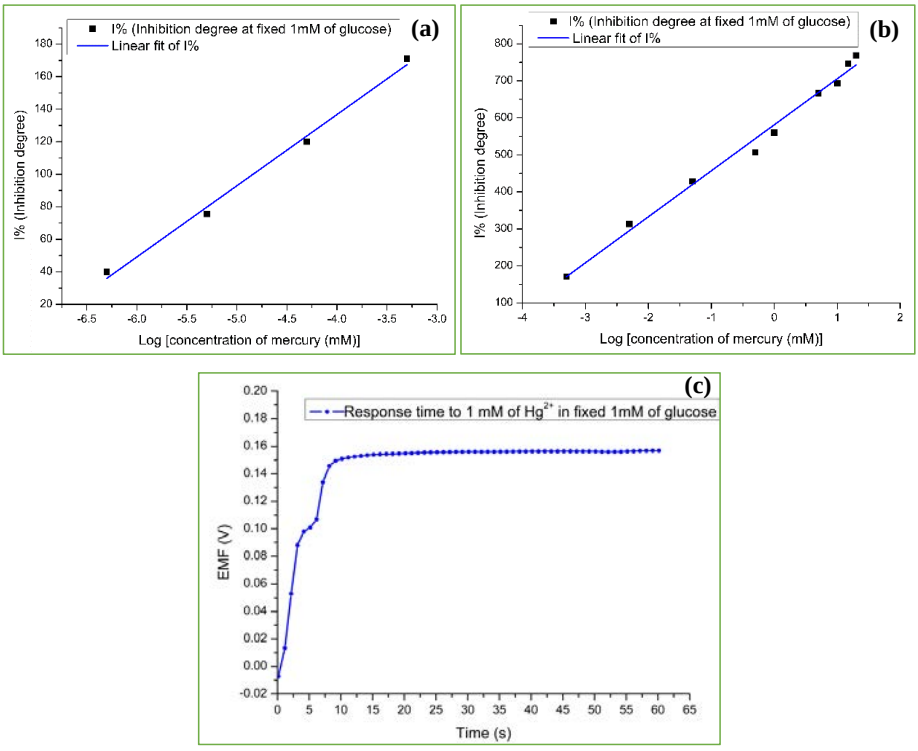

Figure 5. 12: *(a-b) Calibration curve for inhibition of mercury ion at low glucose concentration and (c) the response time of the biosensor to Hg^{2+} ions [18].*

5.2 Synthesis, characterization of TM-doped ZnO nanostructures and their sensing applications

5.2.1 Low temperature synthesis, structural, and optical properties of Mn-doped ZnO nanostructures (Paper V)

As mentioned in the previous chapter, introducing TM into the ZnO matrix can improve its electrical and optical properties, and enhances the room temperature ferromagnetism, which makes the TM-doped ZnO nanostructures to be of potential. This work presents the hydrothermal growth of Mn-doped ZnO nanostructures by an adopted procedure used for un-doped ZnO nanowires described in [6]. In this method, the substrate preparation and seeding process were done in same way as described in session 5.1.2 above. For homogenous solution preparation process, firstly, an aqueous solution *A* is prepared by mixing equimolar 0.075 M of zinc nitrate hexahydrate and HMT in DI water. Secondly, solution *B* is the Mn ions solution prepared by dissolving a specific percentage (1% and 5%) of $MnCl_26H_2O$ in DI water containing 20% of ethanol. Thirdly, solutions *A* and *B* were mixed and homogenized by ultrasonication bath for another one hour. Finally, the mixed solution was subsequently stirred at RT for one hour. For the hydrothermal growth process, the ZnO seed-layers coated substrates were placed horizontally in the growth solution and kept in a preheated oven for 5 hours at 80^{o}C. Figures 5.13 (a-c) show the SEM images of ZnO NWs, 1% Mn-doped ZnO sample and 5% Mn-doped ZnO sample. It can clearly be seen that the surface morphology of the ZnO changed from nanowires-like to nano-disc-like while the Mn concentration reached 5.0%. The chemical composition and electronic structure of the 5% Mn doped sample have been performed by EDX and XPS spectroscopies, respectively. Figure 5.13 (d) shows the EDX peaks of Mn ions at 0.56, 0.63, 5.89 and 6.49 keV. It indicates that the Mn ions was present in the ZnO sample.

Figure 5.14 (a) shows the XPS spectrum of the 5% Mn-doped ZnO sample. Figure 5.14 (b) shows two strong XPS peaks at 1022.5 eV and 1045.5 eV of binding energy. These peaks correspond to the energies of the Zn $2p_{3/2}$ and the Zn $2p_{1/2}$, respectively. While the XPS peaks at a binding energy of 531.3 eV belong to the peak of the O 1s (Figure 5.14-c). Figure 5.14 (d) shows two weak XPS peaks at binding energies of 641.7 and 657.3 eV, which is corresponded to the binding energies of Mn $2p_{3/2}$ and Mn $2p_{1/2}$, respectively [20-22]. These results indicated that there are small amount of Mn^{2+} incorporated into the ZnO matrix, which is the Mn^{2+} valence state replacing some of the Zn ions in the $Zn_{0.95}Mn_{0.05}O$ NWs. Figure 5.15 (a) shows that the (002) peaks of 1% Mn-doped ZnO sample and 5% Mn-doped ZnO sample were shifted

to lower 2θ values and the FWHM was larger while increasing the manganese concentration. This shift is due to the difference in ionic radii of Mn^{2+} (~0.66 Å) and Zn^{2+} (~0.60 Å) which indicated that the Mn ions were incorporated into the ZnO crystal lattice. Figure 5.15 (b) presents the room temperature PL emission of 5% Mn doped ZnO sample. The two dominated peaks of UV emission centered at 378 nm (3.28 eV) and a sharp peak of visible region centered at 529 nm (2.34 eV) were observed. The PL emission peak at the visible region is different with the peaks of the undoped ZnO NWs samples which possesses a broad emission peaks around 529 nm. This is due to the absence of some oxygen vacancy caused by the incorporation of Mn ion into the ZnO matrix [23].

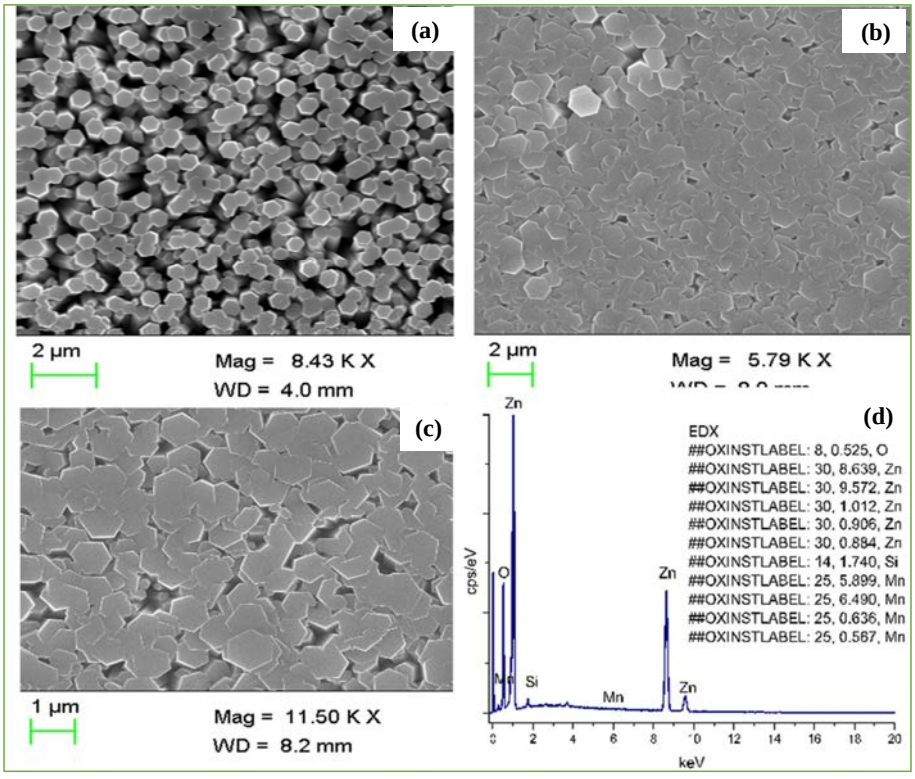

Figure 5. 13: *The SEM images (a) ZnO NWs (b) 1% Mn-doped ZnO NWs (c) 5% Mn-doped ZnO sample and (d) EDX spectrum of 5% Mn-doped ZnO sample [23].*

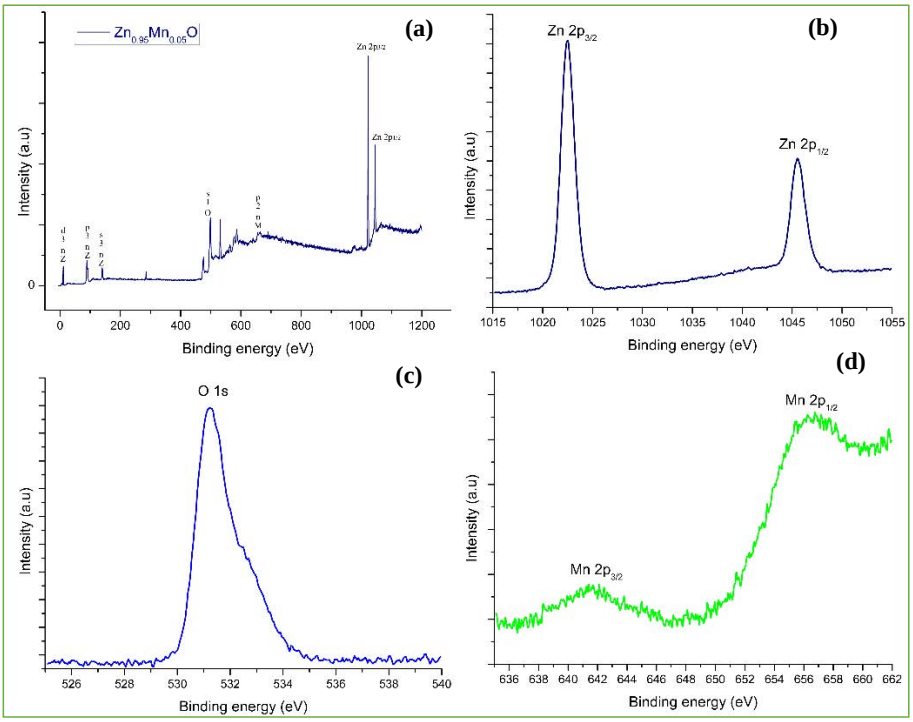

Figure 5. 14: *The XPS spectra (a) 5% Mn-doped ZnO (b) Zn 2p (c) O1s and (d) Mn 2p [23].*

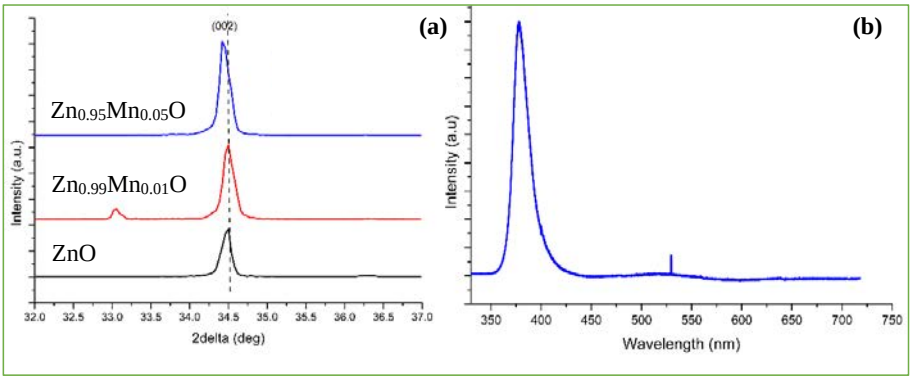

Figure 5. 15: *(a) The XRD patterns the (002) peaks of undoped ZnO and Mn-doped ZnO samples and (b) the room temperature PL spectrum of 5% Mn-doped ZnO sample [23].*

5.2.2 Fast piezoresistive sensor and UV photodetector based on Mn-doped ZnO NRs (Paper VI)

Synthesis of Mn-doped ZnO NRs with controlled size, structure, and uniformity on any substrates remains big a challenge. In this work, Mn-doped ZnO NRs were synthesized by a new and simple method which was adopted by using ammonia as a source of OH^- instead of HMT, which maintains the structures with high incorporation of Mn dopant concentration in the ZnO matrix [24]. The synthesized Mn-doped ZnO nanorods was fabricated as Schottky diode and used for fast piezoresistive sensor and UV photodetector.

The growth procedure is performed by mixing a 0.075 M of zinc nitrate hexahydrate and 15% atomic concentration of manganese nitrate hexahydrate in DI water for 2 hours. Then ammonia solution is rapidly injected into the mixture solution under stirring, which makes the growth solution to have a pH = 10. Finally, the mixed solution was kept under stirring for 30 minutes at room temperature. The growth process was performed typically by horizontally placing the prepared ZnO seed-layers coated substrates in the growth solution and they kept in a preheated oven at 90^o C for 6 hours. The experimental results shows that the surface morphology of the ZnO NRs and the $Zn_{0.85}Mn_{0.15}O$ NRs have hexagonal shapes with diameters varying between 250-350 nm as in Figure 5.16.

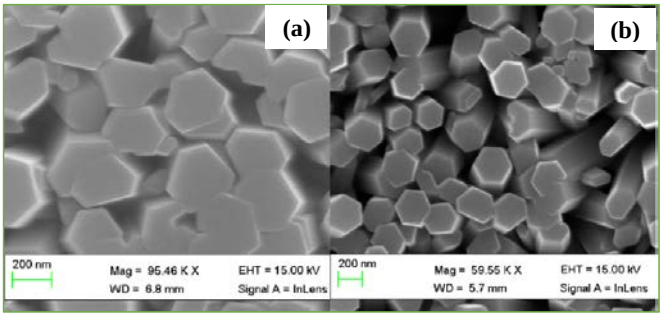

Figure 5. 16: *(a) SEM image of ZnO NRs and (b) SEM image of $Zn_{0.85}Mn_{0.15}O$ NRs [24].*

To investigate the structure and the existence of the Mn^{2+} ions substituted in the lattice position of Zn site, the XRD and XPS spectroscopies were used. Figure 5.17 (a-b) show XRD patterns of ZnO NRs and $Zn_{0.85}Mn_{0.15}O$ NRs. The diffraction peaks of $Zn_{0.85}Mn_{0.15}O$ sample shows that the sample grows along the *c-axis* without any impurity phases such as metallic manganese or manganese oxides that have been observed. Its (002) peak position was shifted and the FWHM was larger in comparison to the (002) peak of the ZnO NRs sample. This indicates that the Mn ions replaced the Zn sites in the ZnO NRs matrix [20]. Figure 5.17 (c)

shows two peaks at 641.15 eV and 657.5 eV, which correspond to the binding energies of Mn $2p_{3/2}$ and Mn $2p_{1/2}$, respectively. These results indicate that Mn^{2+} ions were incorporated into the ZnO NRs crystal matrix [20-26]. A comparison of UV-vis absorption spectra of ZnO NRs and Mn-doped ZnO NRs are shown in Figure 5.17 (d). In the UV region, the absorption intensity of the Mn-doped ZnO sample was higher and shifted towards lower wavelength compared to ZnO NRs. This blueshift can be explained by the Burstein-Moss effect [27].

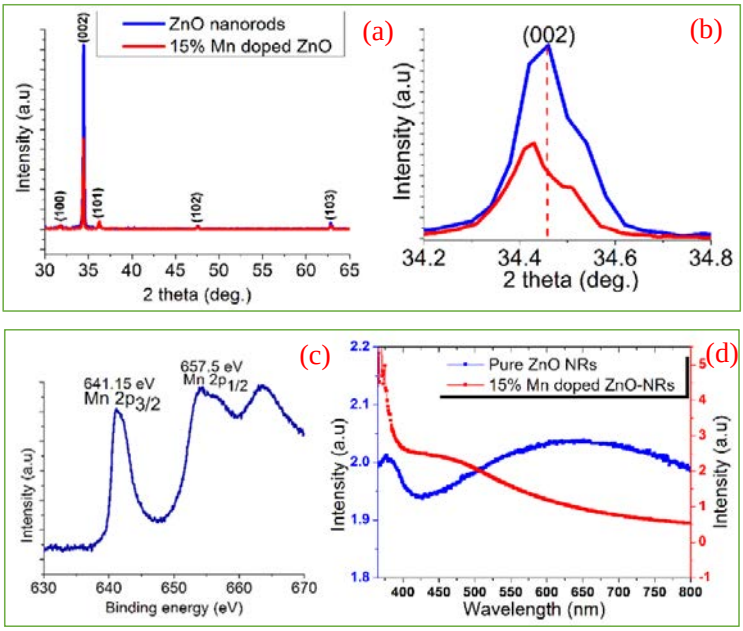

Figure 5. 17: *(a-b) XRD pattern of ZnO and $Zn_{0.85}Mn_{0.15}O$ NRs (c) the XPS spectrum of the Mn2p and (d) the UV-vis absorption spectra of ZnO and $Zn_{0.85}Mn_{0.15}O$ NRs [24].*

Figure 5.18 (a) shows the *I-V* characteristic of the device under both dark and UV illumination of 2 mW/cm^2 with a wavelength of 365 nm and the inserted graph shows the time response. The responsivity value was calculated under 5V of forward bias to be 0.065 A/W and response times was found to be about 2.75s. The Schottky diode also works as piezoresistive sensor. Figure 5.18 (b) shows the *I-V* characteristics of the fabricated piezoresistive sensor under different applied loads ($m_8 > m_7 > \ldots > m_1$) with the insert showing a schematic diagram of the device and its response time. The fabricated sensor shows good reliability with relatively fast response and recovery times of ~0.03s and ~0.27 s, respectively. The device shows electronic resistance variation ratios versus the applied loads can be divided into two linear

parts, the first linear range is up to 20 KPa with pressure sensitivity (S) of 0.00617 KPa^{-1} and the second linear range is from 20 KPa to 320 KPa with S = 0.000180 KPa^{-1} (Figure 5.18 c-d).

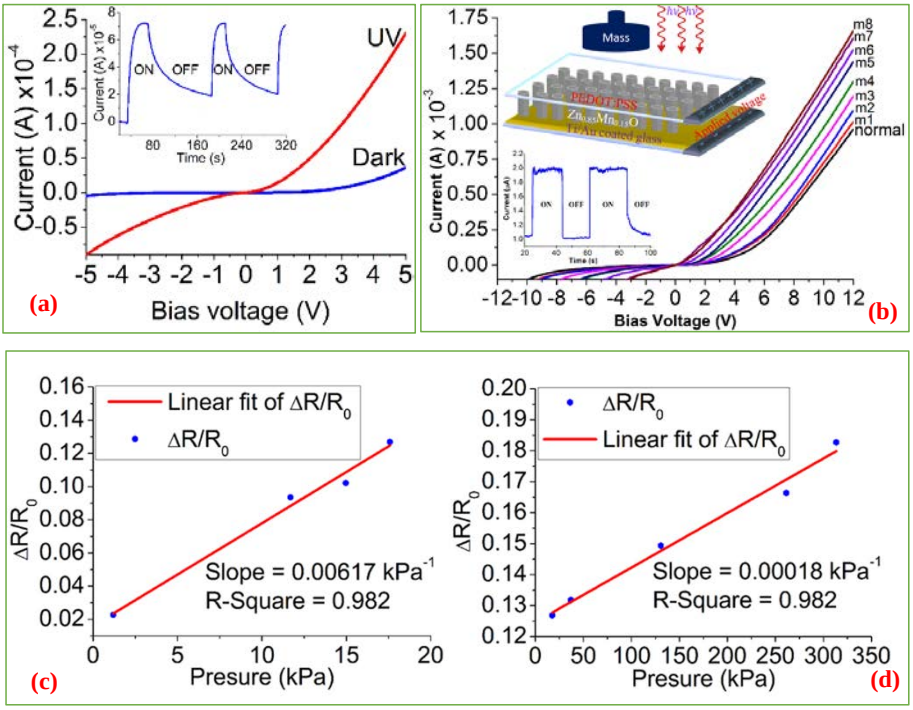

Figure 5. 18: *(a) I-V characteristics of the Mn-doped ZnO Schottky diode based UV photodetector and the inserted its response time, (b) I-V characteristics of the piezoresistive sensor based device under external applied loads, the inserted schematic diagram of the device and the response time and (c-d) the electronic resistance variation ratios of the piezoresistive sensor [24].*

5.2.3 Synthesis of Fe-doped ZnO NRs by rapid mixing hydrothermal approach and its high performance UV photodetector (Paper VII)

We believe that by introducing TM into the ZnO nanomaterial we can possibly enhance the room temperature ferromagnetic properties. We also believe that Fe-doped ZnO NRs can be useful for many nanotechnology applications, including nanoelectronics, optoelectronics, spin electronics applications and sensor devices [28-30]. In this work, the synthesis method developed to grow Fe-doped ZnO NRs represents a new and simple method. The synthesized Fe-doped ZnO NRs were used to fabricate a simple Au/Fe-doped ZnO Schottky diode UV photodetector. In this growth method, ($ZnNO_3 \cdot 6H_2O$), ($FeCl_2 \cdot 4H_2O$) and ($FeCl_3 \cdot 6H_2O$) were used as source materials. The growth solution was prepared by one hour mixing of 0.075 M

of ($ZnNO_3 \cdot 6H_2O$) and a specific amount of iron ions with the ratio of [Fe^{+2}: Fe^{+3}=1:2] in DI water. Then ammonia solution is added dropwise to the above solution to reach a pH of 9.3 and kept under stirring for another hour at room temperature. Finally, the prepared ZnO seed-layer coated substrates were placed horizontally in the growth solution and kept in a preheated oven for 6 hours at 90^o C. The UV photodetector Schottky device was fabricated by gently pressing a transparent FTO film on top of the 5% Fe-doped ZnO NRs grown on gold coated glass. The XRD measurement and XPS spectroscopy were used to investigate the structure and electronic structures of the grown samples, respectively. The SEM and SQUID were performed to investigate the surface morphology and the room temperature ferromagnetic properties of the Fe-doped ZnO samples. Figure 5. 19 (a) shows the XRD patterns of ZnO NRs, 1% and 5% Fe-doped-ZnO NRs. It is noted that Fe-doped ZnO samples possess hexagonal wurtzite structure and grown along the *c-axis* and there is no secondary phase of irons or iron oxides have been observed. Furthermore, the peaks position at the (002) peak were shifted towards higher diffraction angle and their FWHM became larger while increasing the iron concentration. Figure 5. 19 (b) shows the binding energy of the Fe 2p signals and the Zn Auger peaks between 695 and 736 eV binding energy for both the ZnO nanorods and the Fe-doped ZnO samples. It can be seen that the Fe related signal in the 1% Fe-doped ZnO sample could not be resolved from the Zn Auger due to its relatively lower intensity. However, the Fe $2p_{1/2}$ and Fe $2p_{3/2}$ peaks located at 725.47 and 711.7 eV are clearly observed in the 5% Fe-doped-ZnO samples [31]. The surface morphologies of the 1% and 5.0% Fe-doped ZnO NRs with diameters varying between 100-300 nm are shown in Figure 5. 20 (a-b). Figure 5.20 (c) shows the room temperature ferromagnetic behavior of the Fe-doped ZnO samples measured by the SQUID technique. The ferromagnetic hysteresis loops are clearly observed in the Fe-doped ZnO samples. The magnetization values were increased from 2.5×10^{-6} emu to 9.1×10^{-6} emu for the 1% and the 5% Fe-doped ZnO NRs, respectively. From these systematic investigations, we can conclude that irons ions were incorporated in the ZnO NRs matrix without much morphological or structural deformations and the room temperature ferromagnetism have been enhanced [31]. Figure 5.21 (a) shows the *I-V* curves of the fabricated Schottky device under dark and under UV illumination. The performance of the UV photodetector was investigated by its responsivity and response time. The responsivity was calculated at 5V forward bias to be 2.33 A/W. Figure 5.21 (b) shows 5s and 29s response and recovery times, respectively.

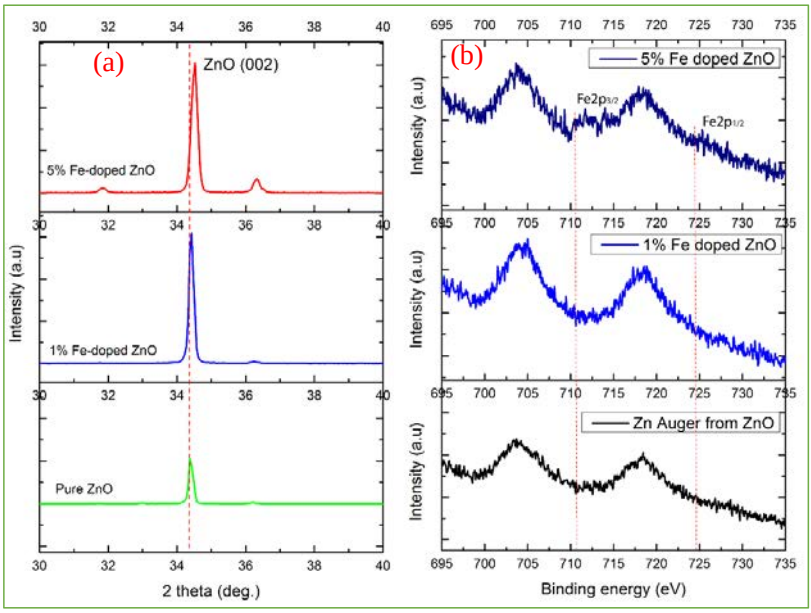

Figure 5. 19: *(a) The XRD patterns of Fe-doped ZnO NRs at (002) peaks and (b) XPS spectra of Zn Auger from ZnO and Fe 2p from Fe-doped ZnO NRs [31].*

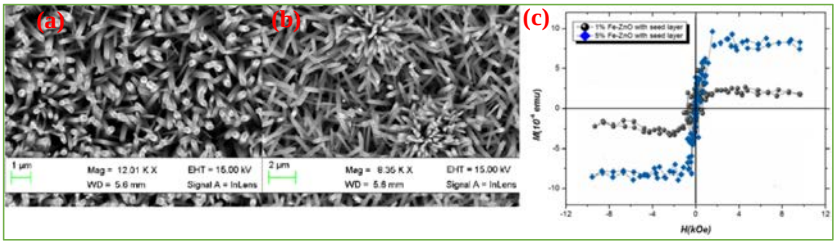

Figure 5. 20: *(a) The SEM images 1% Fe-ZnO NRs (b) the SEM image of 5% Fe-doped ZnO NRs and (c) room temperature ferromagnetic for Fe-doped ZnO NRs [31].*

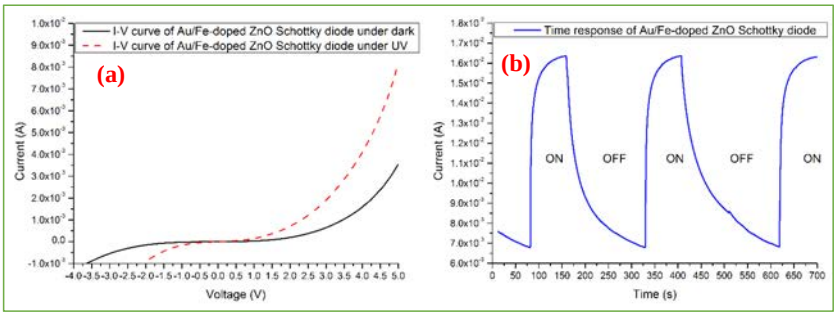

Figure 5. 21: *(a) I-V characteristics of the fabricated Schottky diode under dark and under UV illumination and (b) its response times [31].*

References

[1] C. N. R. Rao, A. Muller, and A. K. Cheetham, Nanomaterials chemistry: Recent developments and new directions, *Wiley-VCH*, Weinheim (2007) p. 140.

[2] A. A. Umar, M. Y. Abd Rahman, R. Taslim, M. M. Salleh and M. Oyama, A simple route to vertical array of quasi-1D ZnO nanofilms on FTO surfaces: 1D-crystal growth of nanoseeds under ammonia-assisted hydrolysis process, *Nanoscale Research Letters* **2011,** 6:564 (12 pages) (2011).

[3] J. H. Tian, J. Hu, S. S. Li, F. Zhang, J. Liu, J. Shi, X. Li, Z. Q. Tian and Y. Chen, Improved seedless hydrothermal synthesis of dense and ultralong ZnO nanowires, *Nanotechnology* **22**, 245601 (9pages) (2011).

[4] C. O. Chey, H. Alnoor, M. A. Abbasi, O. Nur, and M. Willander, Fast synthesis, morphology transformation, structural and optical properties of ZnO nanorods grown by seed-free hydrothermal method, *Phys. Status Solidi A* **211**,No.11, 2611-2615 (2014).

[5] Z. L. Wang, ZnO nanowire and nanobelt platform for nanotechnology, *Materials Science and Engineering R* **64**, 33-71 (2009).

[6] G. Amin, M. H. Asif, A. Zainelabdin, S. Zaman, O. Nur, and M. Willander, Influence of pH, precursor concentration, growth time, and temperature on the morphology of ZnO nanostructures grown by the hydrothermal method, *Journal of Nanomaterials* **Vol. 2011**, Article ID 269692 (9 pages) (2011), doi:10.1155/2011/269692.

[7] S. Xu and Z. L. Wang, One-dimensional ZnO nanostructures: Solution growth and functional properties, *Nano Res.* **4(11)**, 1013-1098 (2011).

[8] L. L. Yang, Q. X. Zhao, M. Willander, Size-controlled growth of well-aligned ZnO nanorod arrays with two-step chemical bath deposition method, *Journal of Alloys and Compounds* **469**, 623-629 (2009).

[9] Q. Li, J. Bian, J. Sun, J. Wang, Y. Luo, K. Sun, D. Yu, Controllable growth of well-aligned ZnO nanorod arrays by low-temperature wet chemical bath deposition method, *Applied Surface Science* **256**, 1698-1702 (2010).

[10] C. O. Chey, S. M. Usman Ali, Z. H. Ibupoto, K. Khun, O. Nur, and M. Willander, Potentiometric creatinine biosensor based on ZnO nanowires, *J. Nanosci. Lett.* **2012**, 2: 24 (2012).

[11] M. Q. Israr, J. R. Sadaf, O. Nur, M. Willander, S. Salman, and B. Danielsson, Chemically fashioned ZnO nanowalls and their potential application for potentiometric cholesterol biosensor, *Appl. Phys. Lett.* **98**, 253705 (2011).

[12] S. M. Al-Hilli, R. T. Al-Mofarji, P. Klason, M. Willander, N. Gutman, and A. Sa'ar, Zinc oxide nanorods grown on two-dimensional macroporous periodic structures and plane Si as a pH sensor, *J. Appl. Phys.* **103**, 014302 (2008).

[13] A. P. Soldatkin, J. Montoriol, W. Sant, C. Martelet, and N. J. Renault, Creatinine sensitive biosensor based on ISFETs and creatinine deiminase immobilised in BSA membrane, *Talanta* **58**, 351-357 (2002).

[14] S. R. Mozaz, M. P. Marco, M. J. Lopez de Alda, and D. Barceló, Biosensors for environmental applications: Future development trends, *Pure Appl. Chem.* **76**, 723-752 (2004).

[15] S. R. Mozaz, M. J. Lopez de Alda, M. P. Marco, D. Barcelo, Biosensors for environmental monitoring A global perspective, *Talanta* **65**, 291-297 (2005).

[16] N. Verma, M. Singh, Biosensors for heavy metals, *BioMetals* **18**, 121-129 (2005).

[17] H. S. Wang, Q. X. Pan and G. X. Wang, A Biosensor based on immobilization of horseradish peroxidase in chitosan matrix cross-linked with glyoxal for amperometric determination of hydrogen peroxide, *Sensors* **5**, 266-276 (2005).

[18] C. O. Chey, Z. H. Ibupoto, K. Khun, O. Nur and M. Willander, Indirect determination of mercury ion by inhibition of a glucose biosensor based on ZnO nanorods, *Sensors* **12**, 15063-15077 (2012).

[19] G. L. Turdean, Design and development of biosensors for the detection of heavy metal toxicity, *International Journal of Electrochemistry* **Vol. 2011**, ID 343125 (15 pages) (2011).

[20] R. R. Prabhakar, N. Mathews, K. B. Jinesh, K. R. G. Karthik, S. S. Pramana, B. Varghese, C. H. Sow, S. Mhaisalkar, Efficient multispectral photodetection using Mn doped ZnO nanowires, *J. Mater. Chem.* **22**, 9678-9683 (2012).

[21] J. Wang, H. Li, Y. Huang, Y. Zhang, Fabrication and optical properties of Mn-doped ZnO nanowires, *Advanced Materials Research* **Vols. 79-82**, 453-456 (2009).

[22] G. Li, Z. J. Min, Effects of doping concentration on properties of Mn-doped ZnO thin films, *Chinese Physics B* **18**, 1674-1056 (2009).

[23] C. O. Chey, O. Nur, M. Willander, Low temperature aqueous chemical growth, structural, and optical properties of Mn-doped ZnO nanowires, *Journal of Crystal Growth* **375**, 125-130 (2013).

[24] C. O. Chey, X. Liu, H. Alnoor, O. Nur, and M. Willander, Fast piezoresistive sensor and UV photodetector based on Mn-doped ZnO nanorods, *Phys. Status Solidi-RRL*, (2014) 1-5, DOI 10.1002/pssr.201409453.

[25] Y. H. Tong, F. Cao, J. T. Yang, P. S. Tang, M. H. Xu, Intra-manganese luminescence in ZnO:Mn^{2+} nanorods prepared by a simple thermal evaporation process, *Materials Letters* **94**, 124-127 (2013).

[26] Y. Guo, X. Cao, X. Lan, C. Zhao, X. Xue, and Y. Song, Solution-based doping of manganese into colloidal ZnO nanorods, *J. Phys. Chem. C* **112**, 8832-8838 (2008).

[27] Y. M. Hao, S.Y. Lou, S. M. Zhou, R. J. Yuan, G. Y. Zhu and N. Li, Structural, optical, and magnetic studies of manganese-doped zinc oxide hierarchical microspheres by self-assembly of nanoparticles, *Nanoscale Research Letters* **7**, 100 (9 pages) (2012).

[28] T. Dietl, Dilute magnetic semiconductors: Functional ferromagnets, *Nature Materials* **2**, 646-648 (2003).

[29] S. J. Pearton, D.P. Norton, M. P. Ivill, A. F. Hebard, J. M. Zavada, W. M. Chen, and I. A. Buyanova, Ferromagnetism in transition-metal doped ZnO, *Journal of Electronic Materials* **36**, 462-471 (2007).

[30] C. Liu, F. Yun, and H. Morkoc, "Ferromagnetism of ZnO and GaN: A Review," *Materials in Electronics* **16**, 555-597 (2005).

[31] C. O. Chey, A. Masood, A. Riazanova, X. Liu, K. V. Rao, O. Nur, and M. Willander, Synthesis of Fe-doped ZnO nanorods by rapid mixing hydrothermal method and its application for high performance UV photodetector, *Journal of Nanomaterials* **Volume 2014**, ID 524530 (9 pages) (2014).

Chapter 6: Summary and future prospects

6.1 Research summary

This dissertation deals with studies on the hydrothermal synthesis of ZnO, Mn-doped ZnO and Fe-doped ZnO nanostructures, their characterization and application for biosensors, piezoresistive sensors and UV photodetectors.

In paper I, we have developed a fast and low cost seed-free hydrothermal synthesis ZnO nanostructures with controllable morphology, size and structure. The samples were grown on large areas of Au and Ag coated glass, p-type Si and flexible PEDOT:PSS substrates. A systematic investigation using SEM, XRD, CL spectroscopy and UV-vis absorption suggested that the ZnO NRs can be grown on any type of substrates and the quality of the ZnO NRs can be tuned by increasing the growth duration.

Since well-aligned and uniform size distribution of the ZnO NRs over a large substrate is needed for large scale production. Therefore in paper II, we have synthesized well-aligned, shape controlled and uniform size distribution of ZnO NRs by using a new rapid mixing hydrothermal method and its development for high sensitivity and very fast response time piezoresistive sensor were demonstrated. This is of potential for industrial, civil and transportation applications. The fabricated piezoresistive sensor can be utilized as a very useful human-friendly interactive electronic device for load detection.

Currently, biosensors are widely used in both clinical health care system and in environmental monitoring applications and due to the fabrication of low cost, simple and easy to use of biosensor device to the users is required. In paper III, we have fabricated a potentiometric creatinine biosensor based on electrostatic immobilization of creatinine deiminase (CD) with a chitosan membrane in conjunction with glutaraldehyde on the surface of the ZnO NWs grown on gold coated glass substrates. The performance of the fabricated biosensor indicated a sensitive, selective, stable, reproducible and fast response time of creatinine biosensor. In paper IV, we have developed a potentiometric glucose biosensor by immobilization of glucose oxidase on ZnO NRs grown on gold coated glass not only used for detection of glucose concentration but also used this glucose biosensor for indirect determination of environmental mercury ions. The detection limit to mercury ion was 0.5 nM and the biosensor shows highly sensitive, selective, stable, reproducible, anti-interference, and fast response time to the mercury ions. The application of the glucose biosensor to indirectly

detect the mercury ions possess several advantages such as inexpensive, minimum hardware required, and suitable for onsite use and can be used by unskilled users.

Since diluted magnetic semiconductors are interesting in many applications of nanotechnology and they can be achieved by introducing transition metals into ZnO nanomaterials, and this results in changing of structural, electrical, optical properties and enhances the room temperature ferromagnetic of TM-doped ZnO nanostructures. Therefore in paper V, we synthesized Mn-doped ZnO nanostructures by a low temperature aqueous chemical growth (ACG) method. A systematic investigations by using SEM, EDX, XRD, XPS and PL spectroscopies showed that the Mn-doped ZnO samples had wurtzite structure and the incorporation of Mn ions into the ZnO matrix without any secondary phases have been achieved. The surface morphology was changed from nanorods-like to nano-disc-like with increasing the dopant concentration.

Since nanorods/nanowires structures is the most promising nanostructure for development of nanotechnology. Therefore in paper VI, we have presented a development of low cost hydrothermal synthesis of Mn-doped ZnO NRs with controllable morphology and structure. Ammonia was used to tailor the ammonium hydroxide concentration instead of using HMT. The Mn-doped ZnO NRs have a hexagonal wurtzite ZnO structure and grow along the c-axis and the Mn ions replaced the Zn sites in the ZnO NRs matrix without any secondary phase and its optical property has been improved in comparison to the undoped ZnO NRs. The fabricated PEDOT:PSS/$Zn_{0.85}Mn_{0.15}O$ Schottky diode used for fast piezoresistive sensor and UV photodetector. In paper VII, this new adopted hydrothermal method by using ammonia instead of HMT have been applied to synthesize Fe-doped ZnO NRs and their RT ferromagnetism was investigated. A SQUID measurements showed that the Fe-doped ZnO NRs possesses RT (300 K) ferromagnetic behavior and the magnetization versus field (*M-H*) hysteresis was increased as the dopant concentration increased. Finally, the fabricated Au/Fe-doped ZnO Schottky diode and used as UV photodetector showed very high responsivity and fast response time.

6. 2 Future prospects

There are still plenty of challenges that need to be investigated for both undoped ZnO and TM-doped ZnO NRs, which can affects their properties such as the influence of the growth parameters such as pH, stirring time, mixing procedure, growth temperature and so on. A further study with more detailed characterization for better understanding the relation between the Mn concentrations and their ferromagnetism in Mn-doped ZnO NRs is needed. Since the

surface morphology, surface area to volume ratio, electrical and optical properties of ZnO NRs influence the performance of the sensors. Therefore, continued research efforts in applying our synthesized ZnO NRs and TM-doped ZnO NRs would open new development for many different types of nanosensors such as chemical and biological sensors. Optoelectronics, photonic devices, and spintronics applications such as spin-based light emitting diodes and spin transistors fabricated on low cost and flexible substrates can be interesting to realize.

Publications